Comparative Thermophysiology of Marine Synechococcus CRD1 Strains Isolated From Different Thermal Niches in Iron-Depleted Areas

Mathilde Ferrieux, Louison Dufour, Hugo Doré, Morgane Ratin, Audrey Guéneuguès, Léo Chasselin, Dominique Marie, Fabienne Rigaut-Jalabert, Florence Le Gall, Théo Sciandra, et al.

Comparative thermophysiology of marine *Synechococcus* CRD1 strains isolated from different thermal niches in iron-depleted areas

1 **Mathilde Ferrieux[1], Louison Dufour[1]§, Hugo Doré[1]§, Morgane Ratin[1], Audrey Guéneuguès[2], Léo**
2 **Chasselin[2], Dominique Marie[1], Fabienne Rigaut-Jalabert[3], Florence Le Gall[1], Théo Sciandra[1],**
3 **Garance Monier[1], Mark Hoebeke[4], Erwan Corre[4], Xiaomin Xia[5], Hongbin Liu[6], David J.**
4 **Scanlan[7], Frédéric Partensky[1] and Laurence Garczarek[1,8]**

5 [1] Sorbonne Université, CNRS, UMR 7144 Adaptation and Diversity in the Marine Environment
6 (AD2M), Station Biologique de Roscoff (SBR), Roscoff, France.

7 [2] Sorbonne Université, CNRS, UMR 7621 Laboratoire d'Océanographie Microbienne (LOMIC),
8 Observatoire Océanologique de Banyuls/mer, Banyuls, France.

9 [3] Sorbonne Université, CNRS, Fédération de Recherche FR2424, Station Biologique de Roscoff,
10 29680, Roscoff, France.

11 [4] CNRS, FR 2424, ABiMS Platform, Station Biologique de Roscoff (SBR), Roscoff, France

12 [5] Key Laboratory of Tropical Marine Bio-resources and Ecology, South China Sea Institute of
13 Oceanology, Chinese Academy of Sciences, Guangzhou 510220, China.

14 [6] Department of Ocean Science, The Hong Kong University of Science and Technology, Hong Kong.

15 [7] University of Warwick, School of Life Sciences, Coventry CV4 7AL, UK.

16 [8] CNRS Research Federation (FR2022) *Tara* Océans GO-SEE, Paris, France.

17 § Current address: Department of Ecology, Evolution and Marine Biology; University of California,
18 Santa Barbara, USA

19

20 *** Correspondence:**
21 Corresponding Author: L. Garczarek

22 **Keywords: Marine picocyanobacteria, *Synechococcus*, CRD1, thermotype, temperature**
23 **adaptation**

24

25 **Abstract**

26 Marine *Synechococcus* cyanobacteria are ubiquitous in the ocean, a feature likely related to their

27 extensive genetic diversity. Amongst the major lineages, clades I and IV preferentially thrive in

28 temperate and cold, nutrient-rich waters, whilst clades II and III prefer warm, nitrogen or phosphorus-

29 depleted waters. The existence of such cold (I/IV) and warm (II/III) thermotypes is corroborated by

30 physiological characterization of representative strains. A fifth clade, CRD1, was recently shown to

31 dominate the *Synechococcus* community in iron-depleted areas of the world ocean and to encompass

32 three distinct ecologically significant taxonomic units (ESTUs CRD1A-C) occupying different thermal

33 niches, suggesting that distinct thermotypes could also occur within this clade.

34 Here, using comparative thermophysiology of strains representative of these three CRD1 ESTUs we

35 show that the CRD1A strain MITS9220 is a warm thermotype, the CRD1B strain BIOS-U3-1 a cold

36 temperate thermotype, and the CRD1C strain BIOS-E4-1 a warm temperate stenotherm. Curiously, the

37 CRD1B thermotype lacks traits and/or genomic features typical of cold thermotypes. In contrast, we

38 found specific physiological traits of the CRD1 strains compared to their clade I, II, III and IV

39 counterparts, including a lower growth rate and photosystem II maximal quantum yield at most

40 temperatures and a higher turnover rate of the D1 protein. Together, our data suggests that the CRD1

41 clade prioritizes adaptation to low-iron conditions over temperature adaptation, even though the

42 occurrence of several CRD1 thermotypes likely explains why the CRD1 clade as a whole occupies

43 most iron-limited waters.

44

45 **INTRODUCTION**

46 Marine picocyanobacteria contribute to the biogeochemical cycling of various elements, most notably

47 carbon, contributing ~25% of ocean net primary productivity, of which the *Synechococcus* genus alone

48 is responsible for about 16% (Flombaum et al., 2013). The large geographic distribution of these

49 organisms, extending from the equator to subpolar waters, is largely attributable to their extensive

50 genetic and functional diversity (Zwirglmaier et al., 2008; Farrant et al., 2016; Doré et al., 2020).

51 Amongst the nearly 20 clades within subcluster (SC) 5.1, the most abundant and diversified

52 *Synechococcus* lineage in oceanic ecosystems (Dufresne et al., 2008; Scanlan et al., 2009; Ahlgren and

53 Rocap, 2012), only four (clades I, II, III and IV) were thought to largely dominate *in situ.* Clades I and

54 IV mainly thrive in temperate and cold, nutrient-rich waters, while clades II and III reside in warm,

55 oligotrophic or mesotrophic areas (Zwirglmaier et al., 2008; Mella-Flores et al., 2011), suggesting the

56 existence of cold (I/IV) and warm (II/III) *Synechococcus* 'thermotypes'. This hypothesis was
57 subsequently confirmed by work demonstrating that strains representative of these different clades
58 exhibit distinct thermal *preferenda* (Mackey et al., 2013; Pittera et al., 2014; Breton et al., 2020; Six et
59 al., 2021), a feature notably linked to differences in the thermostability of light-harvesting complexes
60 (Pittera et al., 2017), lipid desaturase gene content (Pittera et al., 2018) and the ability of some strains
61 to induce photoprotective light dissipation at colder temperatures using the orange carotenoid protein
62 (OCP; Six et al., 2021). Field studies using global ocean datasets have allowed to refine the respective
63 ecological niches of the different thermotypes, with clade I extending further north than clade IV
64 (Paulsen et al., 2016; Doré et al., 2022) and clades II and III predominating in N- and P-depleted waters,
65 respectively, but also to highlight the importance of a fifth clade within SC 5.1, the CRD1 clade
66 (Farrant et al., 2016; Sohm et al., 2016; Kent et al., 2019). Initially thought to be limited to the Costa
67 Rica dome area (Saito et al., 2005; Gutiérrez-Rodríguez et al., 2014), the latter clade was recently found
68 to be a major component of *Synechococcus* communities in Fe-depleted areas (Farrant et al., 2016;
69 Sohm et al., 2016; Ahlgren et al., 2020). Furthermore, analysis of the global distribution of these
70 organisms using high-resolution marker genes has highlighted large within-clade microdiversity
71 associated with niche differentiation in marine *Synechococcus* (Farrant et al., 2016; Larkin and
72 Martiny, 2017; Xia et al., 2019), as also observed in *Prochlorococcus* (Kashtan et al., 2014; Larkin et
73 al., 2016). Using the *petB* gene encoding cytochrome b_6, Farrant et al. (2016) showed that most major
74 clades encompassed several Ecologically Significant Taxonomic Units (ESTUs), i.e. genetically
75 related subgroups within clades occupying distinct oceanic niches. This is notably the case for ESTU
76 IIB that occupies a cold thermal niche in sharp contrast with IIA, the dominant ESTU within clade II
77 that occupies warm, mesotrophic, and oligotrophic iron (Fe)-replete waters. Similarly, three distinct
78 ESTUs with distinct thermal niches were identified within the CRD1 clade and the co-occurring clade
79 EnvB (a.k.a. CRD2; Ahlgren et al., 2020): i) CRD1B/EnvBB are found in cold mixed waters in co-
80 occurrence with ESTUs IA, IVA and IVC, ii) CRD1C/EnvBC dominate in warm, high-nutrient low-
81 chlorophyll (HNLC) regions such as the central Pacific Ocean, and iii) CRD1A/EnvBA are present in
82 both environments and thus span a much wider range of temperatures than CRD1B and C (Farrant et
83 al., 2016). This suggests that these three CRD1 ESTUs could correspond to different thermotypes.

84   In order to test this hypothesis, we used strains representative of each of the three CRD1 ESTUs to
85 determine the fundamental thermal niches of these organisms as compared to typical cold (clades I and
86 IV) and warm (clades II and III) thermotypes. Furthermore, given the strong influence of temperature

87   on optimal functioning of the photosynthetic apparatus in marine *Synechococcus* (Pittera et al., 2014,

88   2017; Guyet et al., 2020), we also examined the effect of temperature acclimation on the

89   photophysiology of CRD1 ESTUs compared to their clade I and IV counterparts and show that CRD1

90   thermotypes actually differ more strongly in this respect to members of clades I-IV than from each

91   other.

MATERIALS AND METHODS

Strains and growth conditions

94   The eight *Synechococcus* spp. strains used in this study were retrieved from the Roscoff Culture

95   Collection (RCC; https://roscoff-culture-collection.org/), including representative strains of the three

96   known CRD1 ESTUs (CRD1A – C) and one or two of each of the four dominant clades in the field

97   (clades I – IV) used as controls (Table 1 and Supplementary Fig. 1). Cells were grown in 50 mL flasks

98   (Sarstedt, Germany) in PCR-S11 culture medium (Rippka et al., 2000) supplemented with 1 mM

99   sodium nitrate. Cultures were acclimated for at least two weeks in temperature-controlled chambers

100   across a range of temperatures dependent on the thermal tolerance of each strain and under a continuous

101   light of 75 µmol photons m^{-2} s^{-1} (hereafter µE m^{-2} s^{-1}) provided by a white-blue-green LED system

102   (Alpheus, France). For each experiment cultures were grown in triplicate, inoculated at an initial cell

103   density of ~3 x 10^6 cells mL^{-1}, and samples harvested daily to measure growth rate and fluorescence

104   parameters as described below.

105   In order to compare the capacity of strains to repair the D1 subunit of photosystem II (PSII; see

106   'Measurement of PSII repair rate' section), cultures grown in 250 ml flasks at 75 µE m^{-2} s^{-1} were

107   acclimated at 18, 22 and 25°C, temperatures at which all strains were able to grow, were subjected to

108   high light stress (375 µE m^{-2} s^{-1}). Exponentially growing cultures were sampled at T0 and after 15, 30,

109   60, and 90 min of stress, before shifting cultures back to the initial light conditions and then sampling

110   again after 15, 30, 60 min and 24h of recovery (R). While D1 repair measurements were performed at

111   all time points, cell concentrations were measured by flow cytometry only at T0, T30min, T90min,

112   R30min and R24h and liposoluble pigment content was determined only at T0.

Flow cytometry

114   Culture aliquots (200 µl) sampled for flow cytometry were fixed using 0.25% (v/v) glutaraldehyde

115   (grade II, Sigma Aldrich, USA) and stored at -80°C until analysis (Marie et al., 1999). Cell

116   concentrations were estimated using a Guava easyCyte flow cytometer (Luminex Corporation, USA)

117 and maximum growth rates (μ_{max}) were calculated as the slope of the linear regression of ln(cell

118 density) *vs.* time during the exponential growth phase. *Synechococcus* cells were identified based on

119 their red (695 nm) and orange (583 nm) fluorescence, proxies for their chlorophyll *a* and phycoerythrin

120 content, respectively. Fluorescence, forward scatter and side scatter values were normalized to that of

121 standard 0.95 µm beads using Guavasoft software (Luminex Corporation, USA).

Fluorescence measurements

123 The maximum PSII quantum yield (F_v/F_M) was estimated using a Pulse Amplitude Modulation

124 fluorimeter (Phyto-PAM II, Walz, Germany) during the exponential growth phase after 10 min dark

125 acclimation followed by addition of 100 µM of the PSII blocker 3-(3,4-dichlorophenyl)-1,1-

126 dimethylurea (DCMU, Sigma-Aldrich, USA; Campbell et al., 1998).

127 The PSII quantum yield was calculated as:

$$F_V/F_M = (F_M\text{-}F_0)/F_M$$

129 where F_0 is basal fluorescence, F_M maximal fluorescence level and F_V variable fluorescence (Campbell

130 et al., 1998; Six et al., 2007).

131 Fluorescence excitation (with emission set at 580 nm) and emission (with excitation set at 530 nm)

132 spectra were generated using a LS-50B spectrofluorometer (Perkin-Elmer, USA) as described in Six

133 et al. (2004). The fluorescence excitation ratio ($Exc_{495:550nm}$) was used as a proxy for the PUB:PEB

134 ratio. Phycobilisome (PBS) rod length and the degree of coupling of the PBS to PSII reaction center

135 chlorophylls was then assessed using fluorescence emission spectra by calculating the phycoerythrin

136 (PE, F_{max} = 565–575 nm) to phycocyanin (PC, F_{max} = 645–655 nm) ratio as well as the PC to PBS

137 terminal acceptor (TA; F_{max} = 680 nm) ratio, respectively (Pittera et al., 2017).

Pigment analyses

139 Triplicate cultures were harvested during the exponential phase when F_v/F_M was maximum for each

140 temperature condition. Cultures (50 mL) were subjected to centrifugation in the presence of 0.01%

141 (v/v) pluronic acid (Sigma-Aldrich, Germany) at 4°C, 14,000 x g for 7 min, using an Eppendorf 5804R

142 (Eppendorf, France). Pellets were resuspended and transferred to 1.5 ml Eppendorf tubes and

143 centrifuged at 4°C, 17,000 x g for 2 min using an Eppendorf 5417R centrifuge (Eppendorf, France).

144 Once the supernatant was removed samples were stored at -80 °C until further analysis. Pigment

145   content was subsequently assessed using calibrated high-performance liquid chromatography (HPLC

146   1100 Series System, Hewlett Packard, St Palo Alto, CA), as previously described (Six et al., 2005).

Measurement of the photosystem II repair rate

148   Each culture acclimated to 75 µE m^{-2} s^{-1} and 18, 22 or 25 °C was split into two new 50 mL flasks

149   (Sarstedt Germany) with one used as a control and the other flask supplemented with lincomycin (0.5

150   mg mL^{-1} final concentration, Sigma-Aldrich, USA) in order to inhibit protein synthesis and thus D1

151   repair (Guyet et al., 2020). Both sub-cultures were then subjected to light stress by exposing cultures

152   to 375 µE m^{-2} s^{-1} continuous light (at the same temperature), and F_V/F_M measured at different time

153   points as described above. The PSII repair rate for each strain at each temperature was determined from

154   the coefficient differences between the exponential curves fitted over the 90 min time course of F_V/F_M

155   measurements for control and +lincomycin samples. This light stress experiment was replicated on

156   four independent cultures.

Determination of the realized environmental niches of major *Synechococcus* ESTUs

158   The realized niches of CRD1 and clades I-IV ESTUs were determined using *petB* reads extracted from

159   metagenomic data from the *Tara* Oceans and *Tara* Polar circle expeditions, the Ocean Sampling Day

160   (OSD; June 21st 2014) campaign, and *petB* metabarcodes from i) various oceanographic cruises

161   (CEFAS, BOUM, Micropolar, RRS Discovery cruise 368 and several in the northwestern Pacific

162   Ocean as detailed in Xia et al., 2017), ii) two individual sampling sites in the Mediterranean Sea

163   (Boussole, Point B) as well as iii) a bi-monthly sampling at the long-term observatory site SOMLIT

164   ("Service d'Observation en Milieu Littoral")-Astan located 2.8 miles off Roscoff between July 2009

165   and December 2011 (Supplementary Table 1).

166   *petB* metagenomic recruitment using the *Tara* Oceans and OSD datasets was performed as described

167   previously (Farrant et al., 2016). *Synechococcus petB* sequences from both metagenomes and

168   metabarcodes were used to define operational taxonomic units (OTUs) at 97% identity using Mothur

169   v1.34.4 (Schloss et al., 2009) that were then taxonomically assigned using a *petB* reference database

170   (Farrant et al., 2016). OTUs encompassing more than 3% of the total *Synechococcus* reads for a given

171   sample were grouped into ESTUs and used to determine the whole temperature range occupied by each

172   of the five major *Synechococcus* ESTUs.

173

174 **Comparative genomics**

175   The Cyanorak *v2.1* information system (http://www.sb-roscoff.fr/cyanorak/; Garczarek et al., 2021)

176   was used to compare the phyletic pattern i.e., the presence/absence pattern of each cluster of likely

177   orthologous genes (CLOG) in each strain, for CRD1 strains and their clades I-IV counterparts for a

178   number of selected genes potentially involved in adaptation to low temperature based on previous

179   literature (see results).

180

181 **RESULTS**

182 **The fundamental thermal niches of CRD1 *vs.* clades I to IV strains**

183   In order to determine the temperature optima and boundary limits of the different CRD1 strains and to

184   compare them to those of typical cold and warm *Synechococcus* thermotypes, representative strains of

185   each of the three CRD1 ESTUs and strains of clades I, II, III and IV were grown over a range of

186   temperatures from 6 to 36°C. The growth responses of all strains to temperature followed a typical

187   asymmetric bell-shaped curve over the selected temperature range (Fig. 1), with a progressive rise in

188   growth rate (μ) until T_{opt} (the temperature associated with maximum μ: μ_{max}) was reached, and a sharp

189   decline above T_{opt}. BIOS-U3-1 (CRD1-B) was able to grow between 12 and 29°C with a T_{opt} at 25°C

190   ($\mu_{max} = 0.78 \pm 0.02$ d^{-1}), a growth pattern most similar to that of the clade IV strain BL107, while the

191   clade I strain MVIR-18-1 was able to grow at much lower temperatures, down to 8°C but could not

192   grow above 25°C (Fig. 1A). MITS9220 (CRD1-A) and BIOS-E4-1 (CRD1-C) displayed thermal

193   growth characteristics more similar to the clade II (A15-62 and M16.1) and III (WH8102) strains,

194   representatives of warm thermotypes (Fig. 1B). While most strains in this category displayed a minimal

195   growth temperature of 16°C, large variations between strains were observed at the highest thermal

196   boundary limit (T_{max}). Maximum growth temperature was obtained for M16.1 (II; T_{max}: 34°C), then

197   A15-62 (II) and WH8102 (III; both with T_{max} at 32°C), MITS9220 (CRD1-A; T_{max}: 31°C) and finally

198   for BIOS-E4-1 (CRD1-C; T_{max}: 30°C). The latter strain also displayed the highest minimal growth

199   temperature (T_{min}: 18°C) and thus possesses the narrowest temperature range for growth of all the

200   strains studied (12°C *vs.* 15-18°C). It is also worth noting that CRD1 strains display a lower maximum

201   growth rate and more generally lower growth rates at most temperatures than their clade I, II, III and

202   IV counterparts.

203

The environmental realized niches of CRD1 *vs.* clades I to IV strains

205 We then compared the fundamental thermal niches of all studied strains, i.e. the whole temperature
206 range over which they can grow in a laboratory setting in the absence of biotic interactions (e.g.
207 competition or predation), with environmental realized niches (*sensu* Pearman et al., 2008) of the
208 corresponding ESTUs. For this, we determined the distribution limits of each of these ESTUs along
209 the *Tara* Oceans and *Tara* Polar circle transects, 203 samples from OSD2014 and additional
210 oceanographic cruises and individual sampling sites, altogether encompassing 413 samples worldwide
211 covering a wide range of temperature conditions (Fig. 1, Supplementary Fig. 2, Supplementary Table
212 1). This made it possible to have much finer estimates of the limits of the thermal niches of the different
213 ESTUs than in the study performed by Farrant et al. (2016), in particular for the cold adapted ESTUs,
214 which were poorly represented in the initial *Tara* Oceans dataset (Supplementary Fig. 2).

215 This analysis showed that the CRD1B ESTU displayed a reduced thermal tolerance range in the
216 environment (14 to 24.5°C) compared to the BIOS-U3-1 strain in culture (12 to 29°C), while the typical
217 cold thermotypes colonized larger thermal niches *in situ* than their representative strains (Fig. 1A).
218 Environmental realized niches indeed ranged from 2.5 to 24°C for ESTU IA (compared to 8 to 25°C
219 for MVIR-18-1) and from 8.5 to 25°C for ESTU IVA (compared to 12 to 29°C for BL107).
220 Interestingly, the median temperature of the CRD1B ESTU is 3°C higher than that observed for ESTUs
221 IA and IVA.

222 As concerns warm thermotypes, CRD1C displayed a fairly narrow thermal tolerance range *in situ*
223 (22 to 29.5°C), which, similar to the cold thermotype CRD1B, was even narrower than for its
224 representative strain BIOS-E4-1 (18 to 30°C; Fig. 1B). Comparatively, the CRD1A ESTU was detected
225 across a wider temperature range (14 to 30.5°C) than the other two CRD1 ESTUs and also slightly
226 larger than the corresponding strain in culture (MITS9220, 16 to 31°C). Still, the most extended
227 temperature range was observed for ESTU IIA and IIIA (12 to 32°C) that reached significantly lower
228 temperature limits than the corresponding clade II (16 to 32-34°C) and III (16 to 32°C) strains. Of note,
229 although both IIA and IIIA ESTUs displayed a similar temperature range, the median temperature of
230 ESTU IIA (25°C) was about 3°C higher than that of ESTU IIIA (22°C) and the maximum median
231 temperature was surprisingly observed for the CRD1C ESTU (26.5°C). In this context, it is also worth
232 mentioning that although clade II strains are clearly both warm thermotypes, M16.1 displays a

233   significantly higher temperature limit for growth than A15-62 and more generally than all other strains.

234   This suggests that ESTU IIA may encompass two distinct ESTUs, but such a high temperature niche

235   (>32 °C) where they could be discriminated is exceptional and not available in our dataset

236   (Supplementary Table 1).

237   **Comparative genomics**

238   In order to assess whether the cold, temperate thermotype BIOS-U3-1 (CRD1B) exhibits similar

239   adaptation mechanisms to those previously described for the cold-adapted clades I and/or IV, we

240   examined a number of clusters of likely orthologous genes (CLOGs) from all *Synechococcus* genomes

241   belonging to clades I-IV and CRD1 present in the Cyanorak *v2.1* information system (Garczarek et al.,

242   2021). First, we looked for the occurrence of two amino-acid substitutions in phycocyanin α- (RpcA)

243   and β-subunits (RpcB), which were shown to differ between cold- (Gly in clades I and IV for RpcA43;

244   Ser in RpcB42) and warm-thermotypes (Ala in clades II and III for RpcA43; Asp in RpcB42), these

245   substitutions being potentially responsible for the differential thermotolerance of this phycobiliprotein

246   between thermotypes (Pittera et al., 2017). In all three CRD1 strains, both sites displayed the warm-

247   type residue (Supplementary Fig. 3A-B), suggesting that in contrast to typical cold and warm

248   thermotypes, the molecular flexibility of this phycobiliprotein does not differ between CRD1

249   thermotypes. We then looked at fatty acid desaturases that are essential for regulating membrane

250   fluidity and thus the activity of integral membrane proteins, including photosynthetic complexes

251   (Mikami and Murata, 2003; Pittera et al., 2018; Breton et al., 2020). All three CRD1 strains surprisingly

252   possess in addition to the core Δ9-desaturase gene *desC3*, a second Δ9-desaturase, *desC4*

253   (Supplementary Table 2), previously thought to be specific to cold-adapted strains as well as the Δ12-

254   desaturase *desA3* found in both cold-adapted clades I and IV as well as in clade III, a warm thermotype

255   subjected to much stronger seasonal variability than its (sub)tropical clade II counterparts (Pittera et

256   al., 2018). Furthermore, BIOS-U3-1 also possesses *desA2*, thought to be specific to warm

257   environments, while this gene is in contrast absent from the other two CRD1 warm-adapted strains.

258   Thus, CRD1 strains exhibit a different desaturase gene set and potentially display a larger capacity to

259   regulate membrane fluidity than typical cold- or warm-adapted thermotypes. Finally, while all clades

260   I, III and IV genomes possess the *ocp* operon, involved in the protection of PSII against

261   photoinactivation through the dissipation of excess light energy (Kirilovsky, 2007) and which was

262   recently shown in marine *Synechococcus* to play a key role at low temperature (Six et al., 2021), none

263   of the three CRD1 genomes possess this operon.

264

Photosynthetic activity and pigment content

266 PSII quantum yield (F_V/F_M), used as a proxy of photosynthetic activity, was measured for each strain

267 over their whole temperature growth range. Most strains displayed a decrease in this parameter at both

268 low and high boundary limits of their growth temperature range and this effect was particularly striking

269 for BIOS-U3-1, reaching values down to 0.11 at 14°C and 0.32 at 28°C (Fig. 2A). Besides MVIR-18-

270 1 that exhibited a quite constant F_V/F_M over its whole temperature range, the decrease in F_V/F_M at high

271 temperature was stronger for cold than warm thermotypes that are able to maintain a quite high F_V/F_M

272 in the warmest growth conditions (Fig. 2B). Finally, as for growth rate, CRD1 strains exhibited lower

273 F_V/F_M at all temperatures than clade I to IV strains.

274 The $Exc_{495:550nm}$ fluorescence excitation ratio, used as a proxy for PUB:PEB ratio, was consistent

275 with the pigment type of each strain (Humily et al., 2013; Table 1; Supplementary Fig. 4A). This ratio

276 remained pretty constant over the whole temperature range for all strains except for the chromatic

277 acclimator BL107 (pigment type 3dA), for which a sharp increase was observed at its maximal growth

278 temperature (28°C) to reach a value (1.35) intermediate between that typically observed in green light

279 (or white light; 0.6-0.7) and blue light (1.6-1.7). This suggests that the chromatic acclimation process

280 could be affected by growth temperature, at least in this strain. The phycobilisome (PBS) rod lengths

281 and the degree of coupling of PBS to PSII reaction center chlorophylls, as estimated from PE:PC and

282 PE:TA ratios respectively, showed fairly limited variations over the temperature range, indicating that

283 the phycobiliprotein composition of PBS is quite stable over the growth temperature range of each

284 strain (Supplementary Fig. 4B-C). One notable exception was a rise in both ratios for strain A15-62 at

285 its minimal growth temperature, likely attributable to the partial decoupling of individual

286 phycobiliproteins and of the whole PBS from PSII, a phenomenon typically observed under stressful

287 conditions (Six et al., 2007; Guyet et al., 2020). It is also worth noting that MITS9220 and to some

288 extent BIOS-E4-1, exhibited a significantly higher PE:PC ratio than the five other strains, potentially

289 indicating a different phycobiliprotein composition and/or length of PBS rods.

290 In terms of liposoluble pigments, the β-carotene/chlorophyll *a* (β-car/Chl *a*) ratio tended to

291 increase with temperature in BIOS-E4-1 and MITS9220, as observed for the other warm thermotypes,

292 whilst this ratio was more stable in the cold thermotypes BIOS-U3-1 and BL107, and seemed to slightly

293 increase in the lower part of the thermal range for the clade I strain MVIR-18-1 (Fig. 3). For all strains,

294   these ratios result from a concomitant increase with temperature of Chl *a* and β-car content per cell

295   (Supplementary Fig. 5), indicating an enhancement of the surface of thylakoids per cell at higher

296   temperatures that was particularly marked for BIOS-E4-1 and A15-62, whilst this variation was fairly

297   limited in the other two CRD1 strains. As these two pigments are present in different proportions in

298   PSI and II (Umena et al., 2011; Xu and Wang, 2017), the higher β-car/Chl a ratio measured in clades

299   I and IV strains also suggests that they may have a higher PSII:PSI ratio than all other strains, including

300   BIOS-U3-1, and that this ratio might be more strongly affected by temperature in warm than cold

301   thermotypes.

302   As concerns the zeaxanthin/chlorophyll *a* (Zea/Chl *a*) ratio, although an increase in this ratio was

303   measured at low temperature for all strains, the amplitude was globally larger for cold than for warm

304   thermotypes, with BIOS-U3-1 behaving very similarly to the clade IV strain BL107 that exhibits the

305   largest variation in this ratio (Fig. 3). Changes in this ratio likely originate partially from the decrease

306   in Chl *a* content in response to cold, a strategy typically used by cells to regulate light utilization under

307   slow growth conditions (Inoue et al., 2001). However, several strains also displayed an increase in their

308   Zea content per cell at low temperature, a response particularly striking in BIOS-U3-1 and A15-62, but

309   that also seems to occur in M16.1 and in the two other CRD1 strains BIOS-E4-1 and MITS9220

310   (Supplementary Fig. 5). Thus, although Zea has been hypothesized to be involved in the

311   photoprotection of cold-adapted strains by dissipating excess light energy under low temperature

312   conditions (Kana et al., 1988; Breton et al., 2020), this process seems to be present in both cold and

313   warm-adapted CRD1 strains and in most warm thermotypes as well. In this context, it is also worth

314   noting that the two clade II strains, A15-62 and M16.1, displayed fairly distinct temperature-induced

315   variations in their Zea:Chl *a* ratios and individual pigment contents, possibly linked to their different

316   isolation temperatures (see discussion below).

317   **Photosystem II repair capacity**

318   The ability of the different strains to repair PSII in response to light stress (375 µE m^{-2} s^{-1}) was

319   determined in cultures acclimated to 18, 22 and 25°C by measuring changes in F_V:F_M over time after

320   adding the protein synthesis inhibitor lincomycin, or not (Supplementary Fig. 6). While a decrease in

321   F_V:F_M ratio during the 90 min light stress period was observed in both cultures supplemented with

322   lincomycin and controls, this ratio only re-increased back up to initial F_V:F_M values, after shifting

323   cultures back to standard light conditions (75 µE m^{-2} s^{-1}), in the control group in most strains and

324   temperature conditions. Thus, all studied strains were able to recover from this light stress, as long as
325   the D1 repair cycle was not inactivated by inhibition of protein synthesis. Yet, a fast decrease in $F_V:F_M$
326   was observed for all three CRD1 cultures supplemented with lincomycin, while the +/- lincomycin
327   curves overlapped during the first 15-30 min of light stress in most other strains and conditions. This
328   suggests that the initial decrease in $F_V:F_M$ in clades I-IV strains was not due to D1 damage but rather
329   to dissipation of light energy as heat through non-photochemical quenching (Campbell et al., 1998),
330   whilst the damage and hence repair of D1 proteins only occurred later on.

331   The PSII repair rate (R_{PSII}), as calculated from the time course of $F_V:F_M$ with and without
332   lincomycin, increased with temperature in most strains, except for BIOS-U3-1 that displayed its highest
333   rate at 22°C (Fig. 4). Strikingly, all three CRD1 strains displayed significantly higher R_{PSII} than clade
334   I-IV strains at all three tested temperatures, a difference ranging from 3- to nearly 40-fold at the lowest
335   common temperature (18°C). Furthermore, CRD1 strains displayed fairly limited variation in R_{PSII} with
336   temperature (ranging from 1.33 to 1.87-fold) compared to the other strains, the strongest increase in
337   R_{PSII} being observed for the clade I strain MVIR-18-1 (21.5-fold) and the clade III strain WH8102 (5.5-
338   fold). This indicates that CRD1 strains exhibit a constitutively high level of PSII repair compared to
339   the other strains whatever the growth temperature and only trigger a moderate increase in R_{PSII} in
340   response to temperature variations.

341

342   **DISCUSSION**

343   Temperature constitutes one the strongest driving factors that have shaped genetic diversification and
344   niche partitioning in marine cyanobacteria (Scanlan et al., 2009; Flombaum et al., 2013; Biller et al.,
345   2015) and phytoplankton at large (Sunagawa et al., 2015; Delmont et al., 2020). While temperature has
346   caused one major diversification event in *Prochlorococcus*, resulting in the divergence of the cold-
347   adapted HLI from the warm-adapted HLII clades (Johnson et al., 2006; Kettler et al., 2007), several
348   independent temperature-related diversification events also occurred in the *Synechococcus* SC 5.1
349   radiation, leading to the emergence of clades I and IV (Dufresne et al., 2008; Zwirglmaier et al., 2008).
350   Here, determination of the temperature optimum and boundary limits (i.e., the fundamental niche) of
351   strains representative of the three CRD1 ESTUs identified in the field (Farrant et al., 2016) showed
352   that different thermotypes can also be delineated within the CRD1 clade, which dominates the
353   *Synechococcus* populations in low-Fe areas of the world Ocean. Comparison with representative strains

354   of the cold-adapted *Synechococcus* ecotypes (clades I and IV) on the one hand, and warm-adapted

355   ecotypes (clades II and III) on the other, made it possible to classify i) the CRD1A strain MITS9220,

356   isolated from the equatorial Pacific Ocean, as a warm thermotype, ii) the CRD1B strain BIOS-U3-1,

357   isolated from the Chilean upwelling, as a cold temperate thermotype, and finally iii) the CRD1C strain

358   BIOS-E4-1, isolated from the edge of the South Pacific gyre, a stable, warm, Fe-depleted oceanic

359   region (Claustre et al., 2008), as a warm temperate stenotherm.

360   As expected from theory (Pearman et al., 2008), the realized environmental thermal niches of

361   CRD1 ESTUs were narrower than their fundamental niches (or similar for MITS9220). In contrast, for

362   ESTUs IA to IVA, the realized environmental niche was significantly more extended towards the low

363   thermal limit than the fundamental niches of their representative strains, this expansion being

364   particularly marked for ESTU IA (Fig. 1). This could be due to passive transport of *Synechococcus*

365   populations by currents into water masses colder than their temperature limits for growth.

366   Alternatively, these ESTUs may exhibit a greater microdiversity than previously assessed (Farrant et

367   al., 2016) and could be subdivided into distinct ESTUs occupying slightly different thermal niches

368   from the current ones, although representative strains to test this hypothesis remain to be isolated. In

369   agreement with the latter hypothesis Paulsen et al. (2016) measured a positive growth rate of

370   *Synechococcus* natural populations dominated by clade I in waters as cold as 2°C in the vicinity of the

371   Svalbard island. Thus, CRD1 ESTUs appear to be strongly outcompeted by their ESTU IA to IVA

372   counterparts at their lower temperature limits. Consistent with this, comparison of their gene content

373   showed that CRD1 ESTUs, including the cold thermotype CRD1B, lack the main adaptation

374   mechanisms reported so far for typical cold thermotypes. Indeed, all CRD1 strains examined in this

375   study i) exhibit warm-type substitutions in their α and β-phycocyanin subunits, influencing the

376   thermotolerance of this phycobiliprotein (Pittera et al., 2017; Supplementary Fig. 3A-B); ii) possess a

377   different set of desaturase genes, involved in regulation of membrane fluidity (Pittera et al., 2018), than

378   typical warm and cold thermotypes (Supplementary Table 2) and iii) lack the OCP system, involved

379   in the protection of PSII against photoinactivation, which seemingly plays a key role at low temperature

380   (Kirilovsky, 2007; Six et al., 2021). Still, we cannot exclude that CRD1 strains could use alternative

381   strategies to cope with temperature variations and notably to deal with the generation of reactive

382   oxygen species, known to be generated by a variety of factors including low and high temperature

383   (Nishiyama et al., 2006; Latifi et al., 2009). For instance, all CRD1 strains possess the *srxA* gene

384   encoding sulfiredoxin catalyzing the reduction of 2-Cys peroxiredoxin involved in H_2O_2 detoxification

385   (Findlay et al., 2005; Guyet et al., 2020) as well as *isiA* that, besides its role in increasing the light-

386   harvesting efficiency of PSI under conditions of Fe-limitation, was also shown to provide

387   photoprotection to PSII by dissipating excess light energy under oxidative stress conditions

388   (Yeremenko et al., 2004; Ihalainen et al., 2005; Supplementary Table 2).

389   The ability of cyanobacteria to grow over a large temperature range largely relies on their capacity

390   to optimize the functioning of their photosynthetic apparatus, notably at low temperature that induces

391   a general slowing down of cell metabolism (Murata et al., 2007; Pittera et al., 2014, 2017). For this

392   reason, we also compared the photophysiology of CRD1 and clades I-IV strains at three growth

393   temperatures common to all strains. These analyses showed that all three CRD1 strains exhibit a lower

394   growth rate at most temperatures than clade I to IV strains (Fig. 1), possibly explaining why they are

395   easily outcompeted by other taxa when iron is no longer limiting, as observed for instance around the

396   Marquesas Islands (Caputi et al., 2019). Moreover, CRD1 strains also display a lower PSII maximum

397   quantum yield (Fig. 2), suggesting that PSII is partially photoinactivated, that is their D1 repair cycle

398   does not fully compensate damage to this protein, even under optimal growth temperatures. Consistent

399   with this, the very high turnover rate of the D1 protein measured in all CRD1 strains indicates that their

400   PSII is much more sensitive to light stress than other strains and can only trigger a moderate increase

401   in R_{PSII} in response to both light and temperature variations, possibly indicating that they are adapted

402   to live deeper in the water column than clades I to IV. This sensitivity could be partially linked to the

403   abovementioned absence of the OCP, potentially reducing their ability to dissipate excess light energy,

404   although it must be noted that the clade II strain A15-62 also lacks the OCP system. Interestingly in

405   this context, all cold thermotypes including the CRD1B strain BIOS-U3-1, possess more copies of the

406   D1:2 isoform (3-6 copies, average: 3.9 ± 1.1) than warm thermotypes (2-3 copies, average: 2.2 ± 0.4),

407   this isoform providing a lower quantum yield but higher PSII resistance to photoinhibition than D1:1

408   (Supplementary Table 2; Clarke et al., 1993a, 1993b; Campbell et al., 1995; Garczarek et al., 2008).

409   Moreover, A15-62 is one of the only *Synechococcus* strains to possess two complete copies of the D1:1

410   isoform, a duplication which could partly explain why, despite the absence of OCP, this atypical clade

411   II strain is able to maintain a high PSII quantum yield over its whole growth temperature range with

412   fairly low D1 repair rates. Interestingly, CRD1 strains also possess a paralog of *psbN*, which was found

413   to be required for the assembly of the PSII reaction centre in *Nicotiana tabacum* and would play an

414   important role in the D1 repair cycle (Torabi et al., 2014).

415   Taken together, both comparative genomics and photophysiological analyses highlighted a
416   number of specificities of CRD1 strains compared to their clade I-IV counterparts, rather than them
417   possessing traits distinctive of cold or warm thermotypes. In this context, it is worth noting that
418   although strains representative of ESTUs IVA and CRD1B exhibit a similar fundamental thermal niche
419   in culture, the higher median temperature of CRD1B in the field indicates that it preferentially thrives
420   in temperate waters (about 18°C, Fig. 1), where energetically costly temperature adaptation
421   mechanisms might not be essential. This suggests that for members of the CRD1 clade, adaptation to
422   low-Fe conditions likely prevails over adaptation to temperature variations, and/or that adaptation
423   mechanisms to temperature variations might be more complex and diversified than previously thought.
424   Still, in terms of a realized environmental thermal niche, the occurrence of several CRD1 thermotypes
425   likely explains why the CRD1 clade as a whole occupies most Fe-limited areas, a vast ecosystem
426   constituting about 30% of the world Ocean (Moore et al., 2013; Bristow et al., 2017). A notable
427   exception is the Southern Ocean, for which from the little available data shows that *Synechococcus* is
428   scarce south of the polar front (Wilkins et al., 2013; Farrant et al., 2016), consistent with the fairly high
429   low-temperature limit (14°C) of the CRD1B environmental realized niche (Fig. 1), while low-Fe
430   availability likely limits the growth of clades I and IV in this area. In contrast, CRD1 growth does not
431   currently appear to be limited by warm temperatures since most oceanic waters display a temperature
432   below 30°C (Supplementary Fig. 2B; Supplementary Table 1). However, one cannot exclude that with
433   global change, some areas of the world Ocean could become warmer than the highest limits determined
434   here for representative strains of CRD1A and C, i.e. 31°C and 30°C respectively. In this context, it is
435   worth mentioning that in the dataset used for this study, several coastal stations, sampled during the
436   OSD campaign reached 31.5 °C (Supplementary Table 1). Thus, although biogeochemistry global
437   models predict that *Synechococcus* could be one of the winners of the phytoplankton community in a
438   future world Ocean (Flombaum et al., 2013; Schmidt et al., 2020; Visintini et al., 2021), it might well
439   not be able to survive in the warmest low-Fe areas, an ecological niche that is currently expanding
440   (Polovina et al., 2008). Although a few studies have started to analyze the genomic bases of adaptation
441   of *Synechococcus* cells to Fe-limitation in the field (Ahlgren et al., 2020; Garcia et al., 2020), further
442   comparative genomic and physiological studies are still needed to decipher the specific capacity of
443   CRD1 clade members to deal with Fe-limitation which should help predict the future distribution and
444   dynamics of *Synechococcus* taxa in the world Ocean.

445

446 **DATA AVAILABILITY STATEMENT**

447 Unpublished metabarcoding data supporting the conclusions of this article are available as raw data

448 (SRA accession numbers) and processed data (number of *petB* reads per ESTU) in Supplementary

449 Table 1. The latter Table also encompasses the description of all environmental samples used in this

450 study.

451

452 **CONFLICT OF INTEREST**

453 The authors declare that the research was conducted in the absence of any commercial or financial

454 relationships that could be construed as a potential conflict of interest.

455

456 **AUTHOR CONTRIBUTIONS**

457 MF, HD and LG designed the experiments. MF, LD, HD, MR, AG, FRJ, TS, LC and GM collected the

458 samples and performed the physiological measurements. MF and DM ran the flow cytometry analyses.

459 FL isolated several CRD1 strains used in this study. HD, XX, DJS, HL and LG performed sequencing

460 and bioinformatics analyses of metabarcodes. MH, EC, FP and LG developed and refined the Cyanorak

461 *v2.1* database. MF, HD, FP and LG made the figures. MF, LD, HD, FP and LG interpreted results. All

462 the authors contributed to the preparation of the manuscript, read and approved the final manuscript.

463

464 **FUNDING**

468

480

481   **SUPPLEMENTARY MATERIAL**

482   **Supplementary Table 1** | Environmental samples used in this study for the determination of the
483   realized environmental niches of the major *Synechococcus* ESTUs

484   **Supplementary Table 2** | Phyletic pattern of CRD1 and clade I-IV genes mentioned in this study
485   retrieved from the Cyanorak v2.1 database

486   **Supplementary Figure 1. Isolation sites of the *Synechococcus* strains used in this study.** Isolation
487   site of each strain is indicated on the map by a bubble arrow colored according to their corresponding
488   ESTUs indicated below the strain name. Longhurst provinces (Longhurst A., 2007, Ecological
489   Geography of the Sea, Academic Press, London) are shown as a colored background shown in the
490   insert. Only provinces from which at least one strain has been isolated are indicated on the map using
491   the following abbreviations: PEQD (Pacific equatorial divergence, Pacific, Trade wind), CHIL (Chile-
492   Peru, current coastal province, Pacific, Coastal), NAST W (Northwest Atlantic subtropical gyral,
493   Atlantic, Westerly), CARB (Caribbean, Atlantic, Trade wind), MEDI (Mediterranean Sea, Atlantic,
494   Westerly), SARC (Atlantic sub-Arctic, Atlantic, Polar).

495 **Supplementary Figure 2. Oceanwide environmental data used in this study to determine the**
496 **environmental realized thermal niches of the main ESTUs from clades CRD1 and I to IV. (A)**
497 Map of the sampling sites, **(B)** Relative abundance of *Synechococcus* ESTUs IA to IVA and CRD1A
498 to C. **(C)** Temperature distribution of the sampling sites. The inserts specify **(A, C)** the name of
499 campaigns or datasets analyzed and **(B)** the *Synechococcus* ESTUs.

500 **Supplementary Figure 3. Alignment of RpcA and RpcB, encoding phycocyanin α- and b-**
501 **subunits, from CRD1 and clades I-IV *Synechococcus* strains. (A)** RpcA. **(B)** RpcB. Substitutions
502 potentially involved in thermotolerance are shown by a red rectangle in the alignment.

503 **Supplementary Figure 4. Variation with growth temperature of phycobilins and**
504 **phycobiliproteins fluorescence excitation and emission ratios. (A)** Average PUB:PEB ratios. **(B)**
505 Average phycoerythrin (PE) to phycocyanin (PC) ratios. **(C)** Average PC to terminal acceptor (TA)
506 ratios. The insert indicates the strain names, their corresponding ESTU (*sensu* Farrant et al., 2016) and
507 pigment type (*sensu* Humily et al., 2013) between brackets.

508 **Supplementary Figure 5. Variation with growth temperature of the three main liposoluble**
509 **pigments per cell for CRD1 vs. clade I and IV strains. (A, D)** Chlorophyll (Chl) *a* content (fg/cell).
510 **(B, E)** Zeaxanthin (Zea) content (fg/cell). **(C, F)** β-carotene (β-car) content (fg/cell). **(A-C)** CRD1-B
511 strain BIOS-U3-1 *vs.* cold thermotypes. **(D-F)** CRD1-A strain MITS9220 and CRD1-C strain BIOS-
512 E4-1 *vs.* warm thermotypes. Inserts indicate the strain names and their corresponding ESTU (*sensu*
513 Farrant et al., 2016) between brackets.

514 **Supplementary Figure 6. Time course of photosystem II quantum yield (F_V/F_M) following light**
515 **stress in the presence or absence of lincomycin for CRD1 and clade I-IV strains acclimated to**
516 **different temperatures.** Cultures acclimated to 75 µE m^{-2} s^{-1} were shifted to 375 µE m^{-2} s^{-1} at T0 for
517 90 min, then shifted back to the initial light conditions for 24h as indicated by a vertical dashed line on
518 each figure. Strain names and their corresponding ESTU between brackets (*sensu* Farrant et al., 2016)
519 are indicated on the right-hand side, acclimation temperatures are indicated on the top, whilst line
520 colour indicates the lincomycin treatment (i.e. -/+ linco).

521

522

REFERENCES

Ahlgren, N. A., Belisle, B. S., and Lee, M. D. (2020). Genomic mosaicism underlies the adaptation of marine *Synechococcus* ecotypes to distinct oceanic iron niches. *Environ. Microbiol.* 22, 1801–1815. doi:10.1111/1462-2920.14893.

Ahlgren, N. A., and Rocap, G. (2012). Diversity and distribution of marine *Synechococcus*: Multiple gene phylogenies for consensus classification and development of qPCR assays for sensitive measurement of clades in the ocean. *Front. Microbiol.* 3, 213–213. doi:10.3389/fmicb.2012.00213.

Biller, S. J., Berube, P. M., Lindell, D., and Chisholm, S. W. (2015). *Prochlorococcus*: The structure and function of collective diversity. *Nat. Rev. Microbiol.* 13, 13–27. doi:10.1038/nrmicro3378.

Breton, S., Jouhet, J., Guyet, U., Gros, V., Pittera, J., Demory, D., et al. (2020). Unveiling membrane thermoregulation strategies in marine picocyanobacteria. *New Phytol.* 225, 2396–2410. doi:10.1111/nph.16239.

Bristow, L. A., Mohr, W., Ahmerkamp, S., and Kuypers, M. M. M. (2017). Nutrients that limit growth in the ocean. *Curr. Biol.* 27, R431–R510. doi:10.1016/j.cub.2017.03.030.

Campbell, D., Hurry, V., Clarke, A. K., Gustafsson, P., and Öquist, G. (1998). Chlorophyll fluorescence analysis of cyanobacterial photosynthesis and acclimation. *Microbiol. Mol. Biol. Rev.* 62, 667–683. doi:10.1128/mmbr.62.3.667-683.1998.

Campbell, D., Zhou, G., Gustafsson, P., Oquist, G., and Clarke, A. K. (1995). Electron transport regulates exchange of two forms of photosystem II D1 protein in the cyanobacterium *Synechococcus*. *EMBO J.* 14, 5457–5466. doi:10.1128/MMBR.62.3.667-683.1998.

Caputi, L., Carradec, Q., Eveillard, D., Kirilovsky, A., Pelletier, E., Pierella Karlusich, J. J., et al. (2019). Community-level responses to iron availability in open ocean plankton ecosystems. *Glob. Biogeochem. Cycles* 33, 391–419. doi:10.1029/2018GB006022.

Clarke, A. K., Hurry, V. M., Gustafsson, P., and Oquist, G. (1993a). Two functionally distinct forms of the photosystem II reaction-center protein D1 in the cyanobacterium *Synechococcus* sp. PCC 7942. *Proc. Natl. Acad. Sci. U. S. A.* 90, 11985–11989. doi:10.1073/pnas.90.24.11985.

Clarke, A. K., Soitamo, A., Gustafsson, P., and Oquist, G. (1993b). Rapid interchange between two distinct forms of cyanobacterial photosystem II reaction-center protein D1 in response to photoinhibition. *Proc. Natl. Acad. Sci. U. S. A.* 90, 9973–9977. doi:10.1073/pnas.90.21.9973.

Claustre, H., Sciandra, A., and Vaulot, D. (2008). Introduction to the special section bio-optical and biogeochemical conditions in the South East Pacific in late 2004: the BIOSOPE program. *Biogeosciences* 5, 679–691. doi:10.5194/bg-5-679-2008.

Delmont, T. O., Gaia, M., Hinsinger, D. D., Fremont, P., Guerra, A. F., Eren, A. M., et al. (2020). Functional repertoire convergence of distantly related eukaryotic plankton lineages revealed by

558   genome-resolved   metagenomics.   *BioRxiv*,   2020.10.15.341214-2020.10.15.341214.
559   doi:10.1101/2020.10.15.341214.

560   Doré, H., Farrant, G. K., Guyet, U., Haguait, J., Humily, F., Ratin, M., et al. (2020). Evolutionary
561   mechanisms of long-term genome diversification associated with niche partitioning in marine
562   picocyanobacteria. *Front. Microbiol.* 11, 567431. doi:10.3389/fmicb.2020.567431.

563   Doré, H., Leconte, Jade, Breton, Solène, Demory, David, Hoebeke, Mark, Corre, Erwan, et al. (2022).
564   Global phylogeography of marine *Synechococcus* in coastal areas unveils strikingly different
565   communities than in open ocean. *BioRxiv*.

566   Dufresne, A., Ostrowski, M., Scanlan, D. J., Garczarek, L., Mazard, S., Palenik, B. P., et al. (2008).
567   Unraveling the genomic mosaic of a ubiquitous genus of marine cyanobacteria. *Genome Biol.*
568   9, R90. doi:10.1186/gb-2008-9-5-r90.

569   Farrant, G. K., Doré, H., Cornejo-Castillo, F. M., Partensky, F., Ratin, M., Ostrowski, M., et al. (2016).
570   Delineating ecologically significant taxonomic units from global patterns of marine
571   picocyanobacteria.   *Proc.   Natl.   Acad.   Sci.   U.   S.   A.*   113,   E3365–E3374.
572   doi:10.1073/pnas.1524865113.

573   Findlay, V. J., Tapiero, H., and Townsend, D. M. (2005). Sulfiredoxin: a potential therapeutic agent?
574   *Biomed. Pharmacother.* 59, 374–379. doi:10.1016/j.biopha.2005.07.003.

575   Flombaum, P., Gallegos, J. L., Gordillo, R. a, Rincón, J., Zabala, L. L., Jiao, N., et al. (2013). Present
576   and future global distributions of the marine Cyanobacteria *Prochlorococcus* and
577   *Synechococcus*. *Proc. Natl. Acad. Sci. U. S. A.* 110, 9824–9829. doi:10.1073/pnas.1307701110.

578   Garcia, C. A., Hagstrom, G. I., Larkin, A. A., Ustick, L. J., Levin, S. A., Lomas, M. W., et al. (2020).
579   Linking regional shifts in microbial genome adaptation with surface ocean biogeochemistry.
580   *Philos. Trans. R. Soc. B Biol. Sci.* 375, 20190254. doi:10.1098/rstb.2019.0254.

581   Garczarek, L., Dufresne, A., Blot, N., Cockshutt, A. M., Peyrat, A., Campbell, D. A., et al. (2008).
582   Function and evolution of the *psbA* gene family in marine *Synechococcus*: *Synechococcus* sp.
583   WH7803 as a case study. *ISME J.* 2, 937–953. doi:10.1038/ismej.2008.46.

584   Garczarek, L., Guyet, U., Doré, H., Farrant, G. K., Hoebeke, M., Brillet-Guéguen, L., et al. (2021).
585   Cyanorak v2.1: a scalable information system dedicated to the visualization and expert curation
586   of marine and brackish picocyanobacteria genomes. *Nucleic Acids Res.* 49, D667–D676.
587   doi:10.1093/nar/gkaa958.

588   Gutiérrez-Rodríguez, A., Slack, G., Daniels, E. F., Selph, K. E., Palenik, B., and Landry, M. R. (2014).
589   Fine spatial structure of genetically distinct picocyanobacterial populations across
590   environmental gradients in the Costa Rica Dome. *Limnol. Oceanogr.* 59, 705–723.
591   doi:10.4319/lo.2014.59.3.0705.

592   Guyet, U., Nguyen, N. A., Doré, H., Haguait, J., Pittera, J., Conan, M., et al. (2020). Synergic effects
593   of temperature and irradiance on the physiology of the marine *Synechococcus* strain WH7803.
594   *Front. Microbiol.* 11, 1707. doi:10.3389/fmicb.2020.01707.

595   Humily, F., Partensky, F., Six, C., Farrant, G. K., Ratin, M., Marie, D., et al. (2013). A gene island
596   with two possible configurations is involved in chromatic acclimation in marine
597   *Synechococcus*. *PLoS One* 8, e84459. doi:10.1371/journal.pone.0084459.

598   Ihalainen, J. A., D'Haene, S., Yeremenko, N., van Roon, H., Arteni, A. A., Boekema, E. J., et al.
599   (2005). Aggregates of the chlorophyll-binding protein IsiA (CP43') dissipate energy in
600   cyanobacteria. *Biochemistry* 44, 10846–10853. doi:10.1021/bi0510680.

601   Inoue, N., Taira, Y., Emi, T., Yamane, Y., Kashino, Y., Koike, H., et al. (2001). Acclimation to the
602   growth temperature and the high-temperature effects on photosystem II and plasma membranes
603   in a mesophilic cyanobacterium *Synechocystis* sp. PCC6803. *Plant Cell Physiol.* 42, 1140–
604   1148. doi:10.1093/pcp/pce147.

605   Johnson, Z. I., Zinser, E. R., Coe, A., McNulty, N. P., Woodward, E. M. S., and Chisholm, S. W.
606   (2006). Niche partitioning among *Prochlorococcus* ecotypes along ocean-scale environmental
607   gradients. *Science* 311, 1737–1740. doi:10.1126/science.1118052.

608   Kana, T. M., Glibert, P. M., Goericke, R., and Welschmeyer, N. A. (1988). Zeaxanthin and ß-carotene
609   in *Synechococcus* WH7803 respond differently to irradiance. *Limnol. Oceanogr.* 33, 1623–
610   1626. doi:10.4319/lo.1988.33.6part2.1623.

611   Kashtan, N., Roggensack, S. E., Rodrigue, S., Thompson, J. W., Biller, S. J., Coe, A., et al. (2014).
612   Single-cell genomics reveals hundreds of coexisting subpopulations in wild *Prochlorococcus*.
613   *Science* 344, 416–420. doi:10.1126/science.1248575.

614   Kent, A. G., Baer, S. E., Mouginot, C., Huang, J. S., Larkin, A. A., Lomas, M. W., et al. (2019). Parallel
615   phylogeography of *Prochlorococcus* and *Synechococcus*. *ISME J.* 13, 430–441.
616   doi:10.1038/s41396-018-0287-6.

617   Kettler, G. C., Martiny, A. C., Huang, K., Zucker, J., Coleman, M. L., Rodrigue, S., et al. (2007).
618   Patterns and implications of gene gain and loss in the evolution of *Prochlorococcus*. *PLoS
619   Genet.* 3, e231. doi:10.1371/journal.pgen.0030231.

620   Kirilovsky, D. (2007). Photoprotection in cyanobacteria: the orange carotenoid protein (OCP)-related
621   non-photochemical-quenching mechanism. *Photosynth. Res.* 93, 7. doi:10.1007/s11120-007-
622   9168-y.

623   Larkin, A. A., Blinebry, S. K., Howes, C., Lin, Y., Loftus, S. E., Schmaus, C. A., et al. (2016). Niche
624   partitioning and biogeography of high light adapted *Prochlorococcus* across taxonomic ranks
625   in the North Pacific. *ISME J.* 10, 1555–1567. doi:10.1038/ismej.2015.244.

626   Larkin, A. A., and Martiny, A. C. (2017). Microdiversity shapes the traits, niche space, and
627   biogeography of microbial taxa: The ecological function of microdiversity. *Environ. Microbiol.
628   Rep.* 9, 55–70. doi:10.1111/1758-2229.12523.

629   Latifi, A., Ruiz, M., and Zhang, C. C. (2009). Oxidative stress in cyanobacteria. *FEMS Microbiol. Rev.*
630   33, 258-278-258–278. doi:10.1111/j.1574-6976.2008.00134.x.

631 Mackey, K. R. M., Paytan, A., Caldeira, K., Grossman, A. R., Moran, D., McIlvin, M., et al. (2013).
632   Effect of temperature on photosynthesis and growth in marine *Synechococcus* spp. *Plant*
633   *Physiol.* 163, 815–829. doi:10.1104/pp.113.221937.

634 Marie, D., Partensky, F., Vaulot, D., and Brussaard, C. (1999). Enumeration of phytoplankton, bacteria,
635   and viruses in marine samples. *Curr. Protoc. Cytom.* 10, 11.11.1-11.11.15.
636   doi:10.1002/0471142956.cy1111s10.

637 Mella-Flores, D., Mazard, S., Humily, F., Partensky, F., Mahé, F., Bariat, L., et al. (2011). Is the
638   distribution of *Prochlorococcus* and *Synechococcus* ecotypes in the Mediterranean Sea affected
639   by global warming? *Biogeosciences* 8, 2785–2804. doi:10.5194/bg-8-2785-2011.

640 Mikami, K., and Murata, N. (2003). Membrane fluidity and the perception of environmental signals in
641   cyanobacteria and plants. *Prog. Lipid Res.* 42, 527–543. doi:10.1016/S0163-7827(03)00036-5.

642 Moore, C. M., Mills, M. M., Arrigo, K. R., Berman-Frank, I., Bopp, L., Boyd, P. W., et al. (2013).
643   Processes and patterns of oceanic nutrient limitation. *Nat. Geosci.* 6, 701–710.
644   doi:10.1038/ngeo1765.

645 Murata, N., Takahashi, S., Nishiyama, Y., and Allakhverdiev, S. I. (2007). Photoinhibition of
646   photosystem II under environmental stress. *Biochim. Biophys. Acta - Bioenerg.* 1767, 414–421.
647   doi:10.1016/j.bbabio.2006.11.019.

648 Nishiyama, Y., Allakhverdiev, S. I., and Murata, N. (2006). A new paradigm for the action of reactive
649   oxygen species in the photoinhibition of photosystem II. *Biochim. Biophys. Acta BBA -*
650   *Bioenerg.* 1757, 742–749. doi:10.1016/j.bbabio.2006.05.013.

651 Paulsen, M. L., Doré, H., Garczarek, L., Seuthe, L., Müller, O., Sandaa, R.-A., et al. (2016).
652   *Synechococcus* in the Atlantic gateway to the Arctic Ocean. *Front. Mar. Sci.* 3, 191.
653   doi:10.3389/fmars.2016.00191.

654 Pearman, P. B., Guisan, A., Broennimann, O., and Randin, C. F. (2008). Niche dynamics in space and
655   time. *Trends Ecol. Evol.* 23, 149–158. doi:10.1016/j.tree.2007.11.005.

656 Pittera, J., Humily, F., Thorel, M., Grulois, D., Garczarek, L., and Six, C. (2014). Connecting thermal
657   physiology and latitudinal niche partitioning in marine *Synechococcus*. *ISME J.* 8, 1221–1236.
658   doi:10.1038/ismej.2013.228.

659 Pittera, J., Jouhet, J., Breton, S., Garczarek, L., Partensky, F., Maréchal, É., et al. (2018).
660   Thermoacclimation and genome adaptation of the membrane lipidome in marine
661   *Synechococcus*. *Environ. Microbiol.* 20, 612–631. doi:10.1111/1462-2920.13985.

662 Pittera, J., Partensky, F., and Six, C. (2017). Adaptive thermostability of light-harvesting complexes in
663   marine picocyanobacteria. *ISME J.* 11, 112–124. doi:10.1038/ismej.2016.102.

664 Polovina, J. J., Howell, E. A., and Abecassis, M. (2008). Ocean's least productive waters are
665   expanding. *Geophys. Res. Lett.* 35, L03618. doi:10.1029/2007GL031745.

666 Rippka, R., Coursin, T., Hess, W., Lichtle, C., Scanlan, D. J., Palinska, K. A., et al. (2000).
667   *Prochlorococcus marinus* Chisholm et al. 1992 subsp. *pastoris* subsp. nov. strain PCC 9511,

668   the first axenic chlorophyll *a*₂/*b*₂-containing cyanobacterium (Oxyphotobacteria). *Int. J. Syst.*
669   *Evol. Microbiol.* 50, 1833–1847. doi:10.1099/00207713-50-5-1833.

670   Saito, M. A., Rocap, G., and Moffett, J. W. (2005). Production of cobalt binding ligands in a
671   *Synechococcus* feature at the Costa Rica upwelling dome. *Limnol. Oceanogr.* 50, 279–290.
672   doi:10.4319/lo.2005.50.1.0279.

673   Scanlan, D. J., Ostrowski, M., Mazard, S., Dufresne, A., Garczarek, L., Hess, W. R., et al. (2009).
674   Ecological genomics of marine picocyanobacteria. *Microbiol. Mol. Biol. Rev.* 73, 249–299.
675   doi:10.1128/MMBR.00035-08.

676   Schloss, P. D., Westcott, S. L., Ryabin, T., Hall, J. R., Hartmann, M., Hollister, E. B., et al. (2009).
677   Introducing Mothur: Open-source, platform-independent, community-supported software for
678   describing and comparing microbial communities. *Appl. Environ. Microbiol.* 75, 7537–7541.
679   doi:10.1128/AEM.01541-09.

680   Schmidt, K., Birchill, A. J., Atkinson, A., Brewin, R. J. W., Clark, J. R., Hickman, A. E., et al. (2020).
681   Increasing picocyanobacteria success in shelf waters contributes to long-term food web
682   degradation. *Glob. Change Biol.* 26, 5574–5587. doi:10.1111/gcb.15161.

683   Six, C., Joubin, L., Partensky, F., Holtzendorff, J., and Garczarek, L. (2007). UV-induced
684   phycobilisome dismantling in the marine picocyanobacterium *Synechococcus* sp. WH8102.
685   *Photosynth. Res.* 92, 75–86. doi:10.1007/s11120-007-9170-4.

686   Six, C., Ratin, M., Marie, D., and Corre, E. (2021). Marine *Synechococcus* picocyanobacteria: Light
687   utilization across latitudes. *Proc. Natl. Acad. Sci.* U. S. A. 118, e2111300118.
688   doi:10.1073/pnas.2111300118.

689   Six, C., Thomas, J., Brahamsha, B., Lemoine, Y., and Partensky, F. (2004). Photophysiology of the
690   marine cyanobacterium *Synechococcus* sp. WH8102, a new model organism. *Aquat. Microb.*
691   *Ecol.* 35, 17–29. doi:10.3354/ame035017.

692   Six, C., Thomas, J.-C., Thion, L., Lemoine, Y., Zal, F., and Partensky, F. (2005). Two novel
693   phycoerythrin-associated linker proteins in the marine cyanobacterium *Synechococcus* sp.
694   strain WH8102. *J. Bacteriol.* 187, 1685–1694. doi:10.1128/JB.187.5.1685-1694.2005.

695   Sohm, J. A., Ahlgren, N. A., Thomson, Z. J., Williams, C., Moffett, J. W., Saito, M. A., et al. (2016).
696   Co-occurring *Synechococcus* ecotypes occupy four major oceanic regimes defined by
697   temperature, macronutrients and iron. *ISME J.* 10, 333–345. doi:10.1038/ismej.2015.115.

698   Sunagawa, S., Coelho, L. P., Chaffron, S., Kultima, J. R., Labadie, K., Salazar, G., et al. (2015).
699   Structure and function of the global ocean microbiome. *Science* 348, 1261359–1261359.
700   doi:10.1126/science.1261359.

701   Torabi, S., Umate, P., Manavski, N., Plöchinger, M., Kleinknecht, L., Bogireddi, H., et al. (2014). PsbN
702   is required for assembly of the photosystem II reaction center in *Nicotiana tabacum*. *Plant Cell*
703   26, 1183–1199. doi:10.1105/tpc.113.120444.

704 Umena, Y., Kawakami, K., Shen, J.-R., and Kamiya, N. (2011). Crystal structure of oxygen-evolving
705   photosystem II at a resolution of 1.9 Å. *Nature* 473, 55–60. doi:10.1038/nature09913.

706 Visintini, N., Martiny, A. C., and Flombaum, P. (2021). *Prochlorococcus*, *Synechococcus*, and
707   picoeukaryotic phytoplankton abundances in the global ocean. *Limnol. Oceanogr. Lett.* 6, 207–
708   215. doi:10.1002/lol2.10188.

709 Wilkins, D., Lauro, F. M., Williams, T. J., Demaere, M. Z., Brown, M. V., Hoffman, J. M., et al. (2013).
710   Biogeographic partitioning of Southern Ocean microorganisms revealed by metagenomics.
711   *Environ. Microbiol.* 15, 1318–1333. doi:10.1111/1462-2920.12035.

712 Xia, X., Cheung, S., Endo, H., Suzuki, K., and Liu, H. (2019). Latitudinal and vertical variation of
713   *Synechococcus* assemblage composition along 170°W transect from the South Pacific to the
714   Arctic Ocean. *Microb. Ecol.* 77, 333–342. doi:10.1007/s00248-018-1308-8.

715 Xu, W., and Wang, Y. (2017). "Function and structure of cyanobacterial photosystem I," in
716   *Photosynthesis: Structures, Mechanisms, and Applications*, eds. H. J. M. Hou, M. M.
717   Najafpour, G. F. Moore, and S. I. Allakhverdiev (Cham: Springer International Publishing),
718   111–168. doi:10.1007/978-3-319-48873-8_7.

719 Yeremenko, N., Kouřil, R., Ihalainen, J. A., D'Haene, S., van Oosterwijk, N., Andrizhiyevskaya, E.
720   G., et al. (2004). Supramolecular organization and dual function of the IsiA chlorophyll-binding
721   protein in cyanobacteria. *Biochemistry* 43, 10308–10313. doi:10.1021/bi048772l.

722 Zwirglmaier, K., Jardillier, L., Ostrowski, M., Mazard, S., Garczarek, L., Vaulot, D., et al. (2008).
723   Global phylogeography of marine *Synechococcus* and *Prochlorococcus* reveals a distinct
724   partitioning of lineages among oceanic biomes. *Environ. Microbiol.* 10, 147–161.
725   doi:https://doi.org/10.1111/j.1462-2920.2007.01440.x.

726

727

728 **TABLES**

729

730 **TABLE 1** | Characteristics of the *Synechococcus* strains used in this study

Strains name	MVIR-18-1	A15-62	M16.1	WH8102	BL107	BIOS-E4-1	BIOS-U3-1	MITS9220
RCC # [1]	2385	2374	791	539	515	2534	2533	2571
Subcluster [2]	5.1	5.1	5.1	5.1	5.1	5.1	5.1	5.1
Clade [2]	I	II	II	III	IV	CRD1	CRD1	CRD1
ESTU [2]	IA	IIA	IIA	IIIA	IVA	CRD1C	CRD1B	CRD1A
Pigment type [3]	3aA	3dB	3a	3c	3dA	3cA	3dA	3dA
Ocean	Atlantic	Atlantic	Atlantic	Atlantic	Med. Sea	Pacific	Pacific	Pacific
Region	North Sea	Offshore Mauritania	Gulf of Mexico	Caribbean Sea	Balearic Sea	South East Pacific	Chile upwelling	Equatorial Pacific
Isolation latitude	61°00' N	17°37' N	27°70' N	22°48' N	41°72' N	31°52' S	34°00' S	0°00' N
Isolation longitude	1°59' E	20°57' W	91°30' W	65°36' W	3°33' E	91°25' W	73°22' W	140°00' W

731 [1]Roscoff Culture Collection, [2]Farrant et al. (2016), [3]Humily et al. (2013).

732

733 **FIGURE LEGENDS**

734

735 **FIGURE 1 │ Fundamental thermal niches of CRD1 *vs.* clade I, II, III and IV strains and environmental**

736 **realized niches of the corresponding ESTUs.** **(A)** CRD1-B strain BIOS-U3-1 *vs.* cold thermotypes. **(B)**

737 CRD1-A strain MITS9220 and the CRD1-C strain BIOS-E4-1 *vs.* warm thermotypes. The insert indicates

738 the strain names and their corresponding ESTU (*sensu* Farrant et al., 2016) between brackets. Each

739 data point is the average of at least 3 biological replicates. Environmental realized niches are indicated

740 as horizontal boxplots for each ESTU above each graph with the whiskers corresponding to 1.5-fold

741 the interquartile range and outliers being plotted as individual points.

742

743 **FIGURE 2 │ Variation with growth temperature of photosystem II quantum yield (F_V/F_M) for CRD1**

744 ***vs.* clade I, II, III and IV strains**. **(A)** CRD1-B strain BIOS-U3-1 *vs.* cold thermotypes. **(B)** CRD1-A strain

745 MITS9220 and the CRD1-C strain BIOS-E4-1 *vs.* warm thermotypes. The insert indicates the strain

746 names and their corresponding ESTU (*sensu* Farrant et al., 2016) between brackets.

747

748 **FIGURE 3 │ Variation with growth temperature of cellular mass pigment ratios of CRD1 *vs.* clade I,**

749 **II, III and IV strains. (A, B)** β-carotene (β-car) to chlorophyll *a* (Chla) ratio. **(C, D)** Zeaxanthin (Zea) to

750 Chl*a* ratio with **(A, C)** CRD1-B strain BIOS-U3-1 *vs.* cold thermotypes and **(B, D)** CRD1-A strain

751 MITS9220 and the CRD1-C strain BIOS-E4-1 *vs.* warm thermotypes. Inserts indicate strain names and

752 their corresponding ESTUs (*sensu* Farrant et al., 2016) between brackets.

753

754 **FIGURE 4 │ Variation with growth temperature of cumulative photosystem II repair rate (RPSII) of**

755 **CRD1 *vs.* clade I, II, III and IV strains**. The insert indicates the strain names and their corresponding

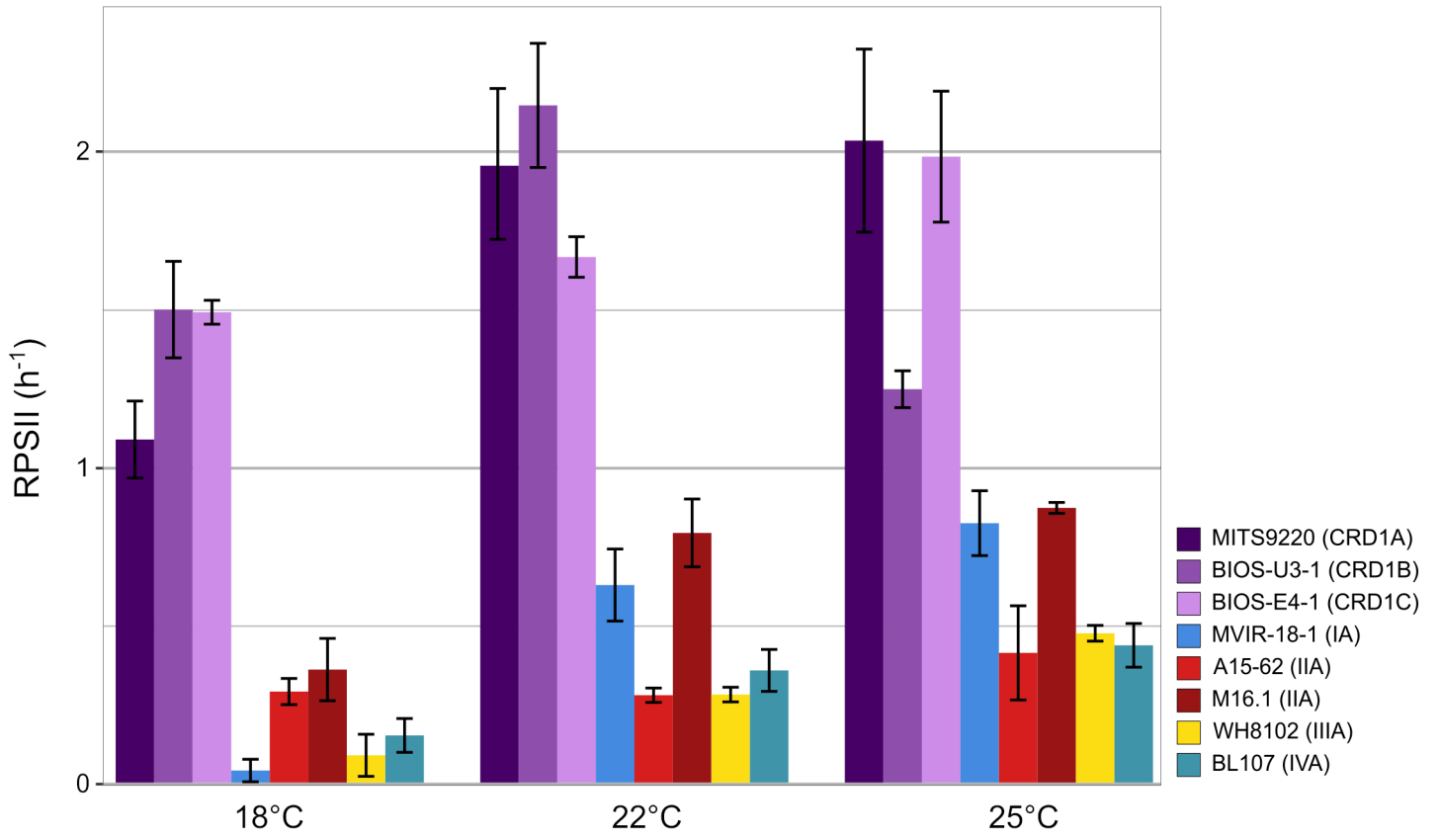756 ESTU (*sensu* Farrant et al., 2016) between brackets.
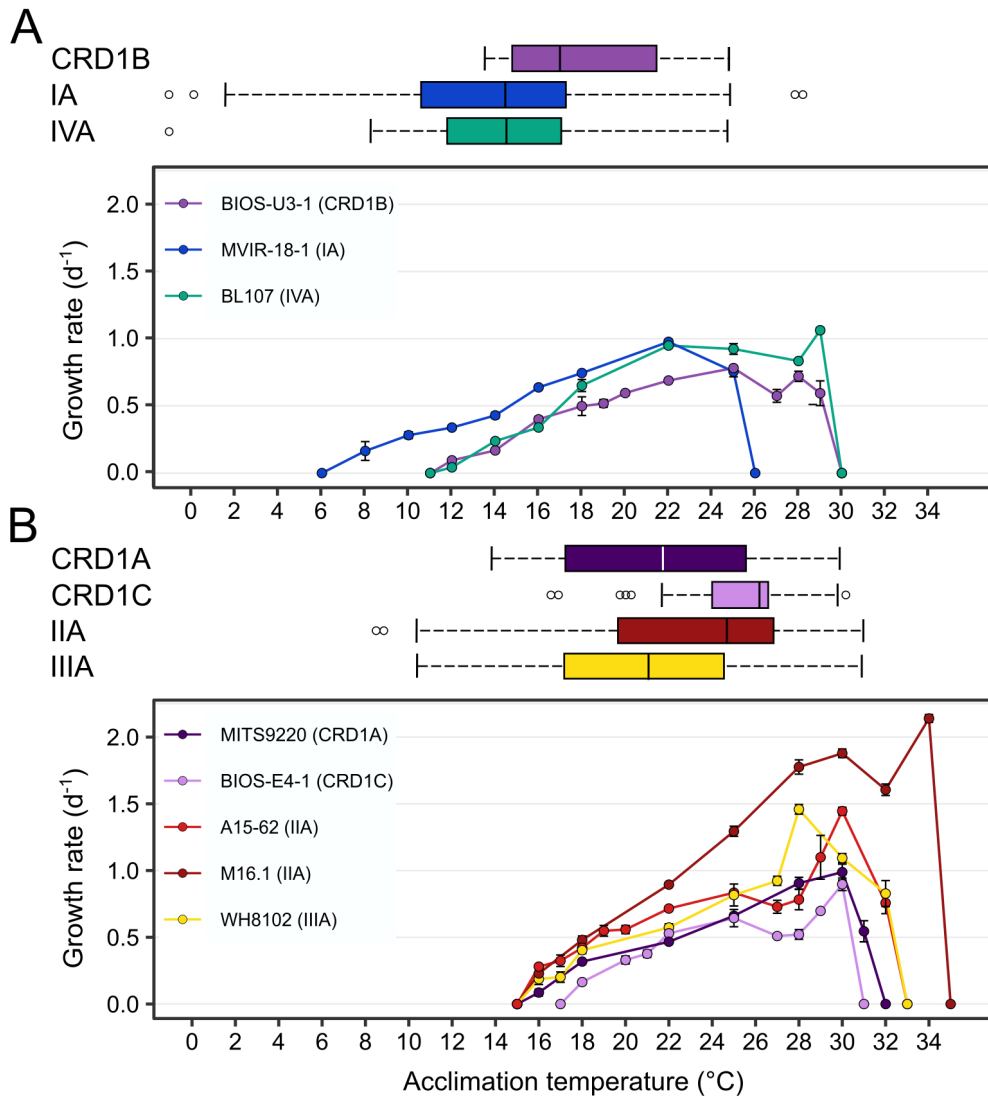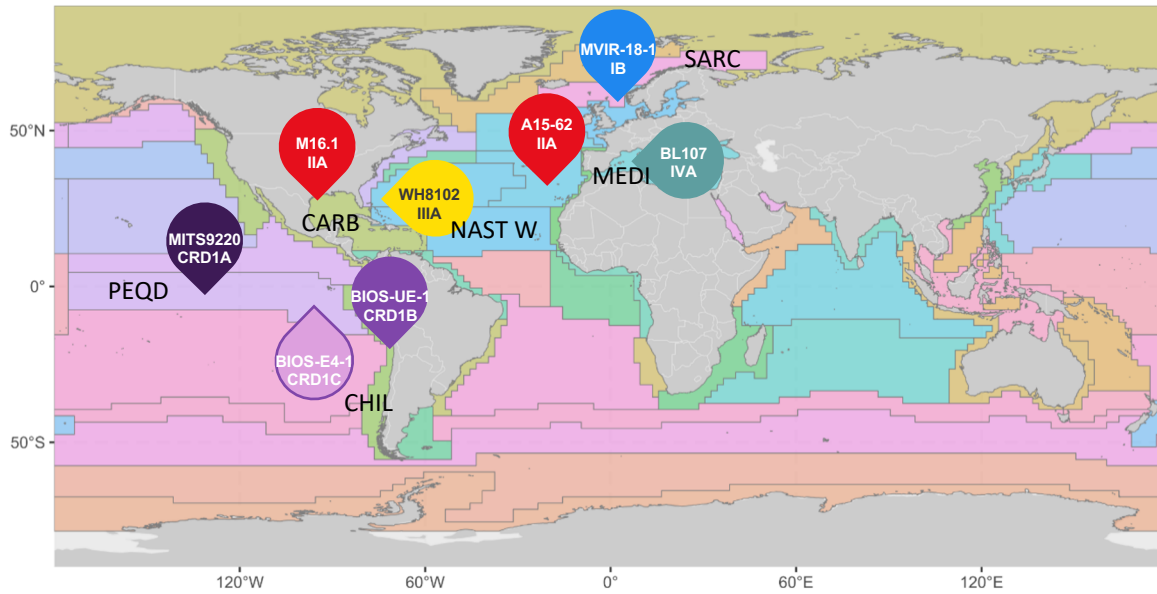
Ferrieux et al., Figure 1
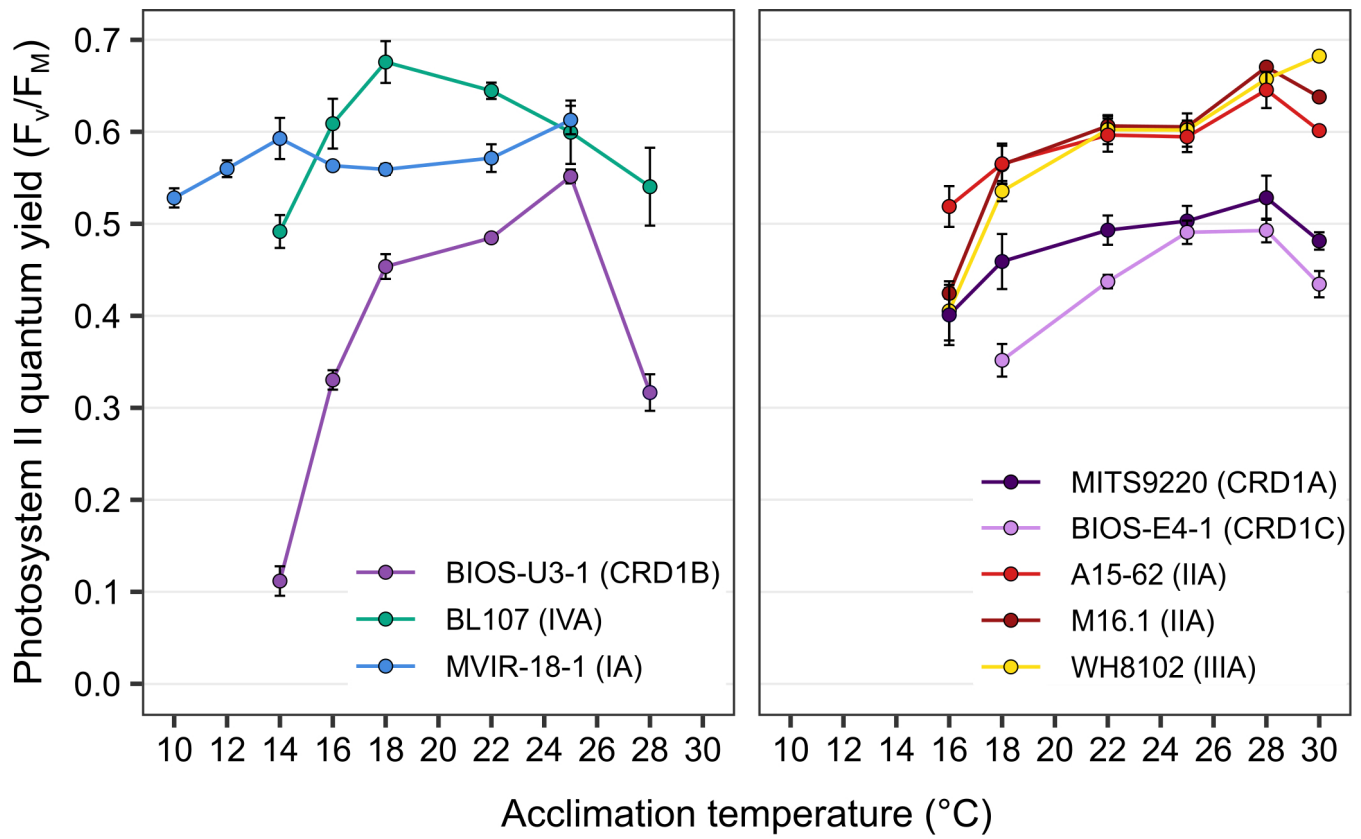
Ferrieux et al., Figure 2
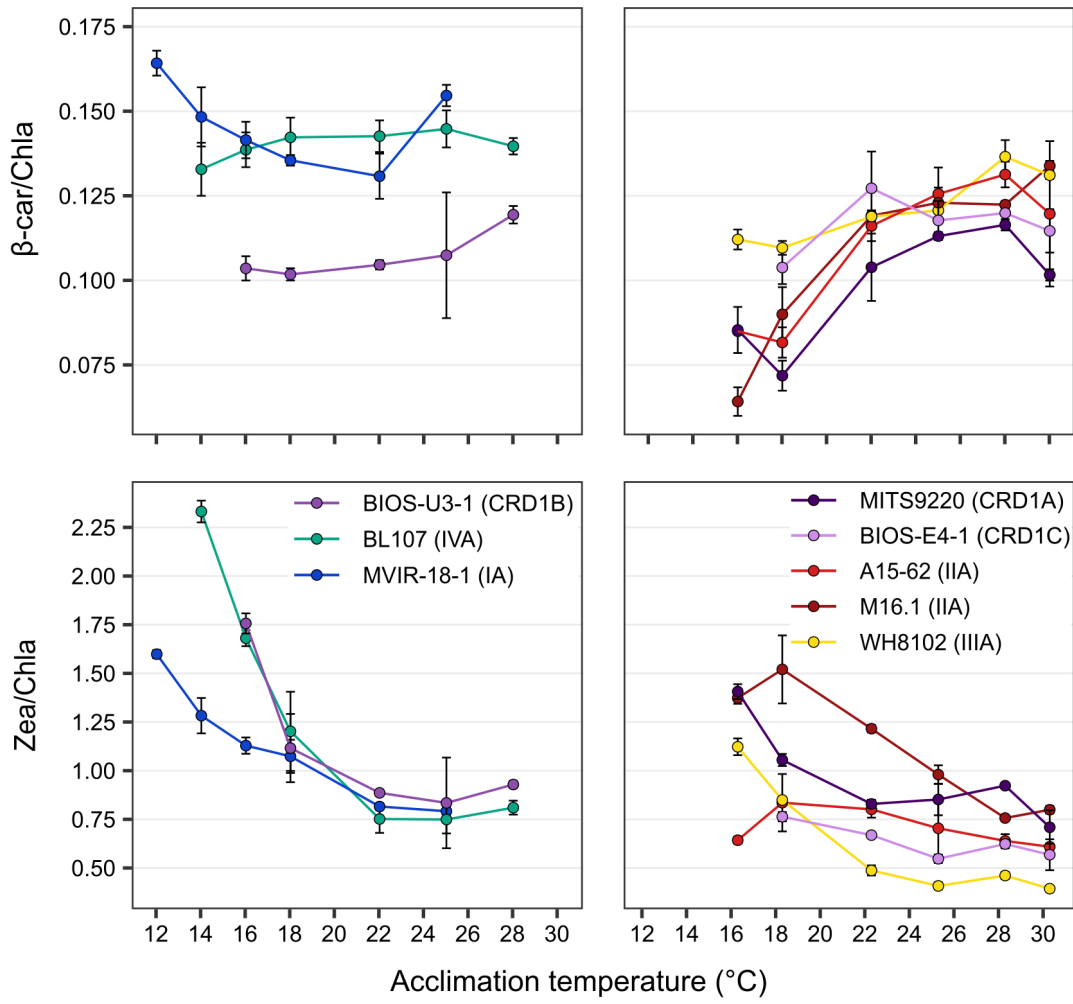
Ferrieux et al., Figure 3

Ferrieux et al., Figure 4

Ferrieux et al.
Supplementary Figures

Supplementary Figure 1. Isolation sites of the *Synechococcus* **strains used in this study.** Isolation site of each strain is indicated on the map by a bubble arrow colored according to their corresponding ESTUs indicated below the strain name. Longhurst provinces (Longhurst A., 2007, Ecological Geography of the Sea, Academic Press, London) are shown as a colored background shown in the insert. Only provinces from which at least one strain has been isolated are indicated on the map using the following abbreviations: PEQD (Pacific equatorial divergence, Pacific, Trade wind), CHIL (Chile-Peru, current coastal province, Pacific, Coastal), NAST W (Northwest Atlantic subtropical gyral, Atlantic, Westerly), CARB (Caribbean, Atlantic, Trade wind), MEDI (Mediterranean Sea, Atlantic, Westerly), SARC (Atlantic sub-Arctic, Atlantic, Polar).
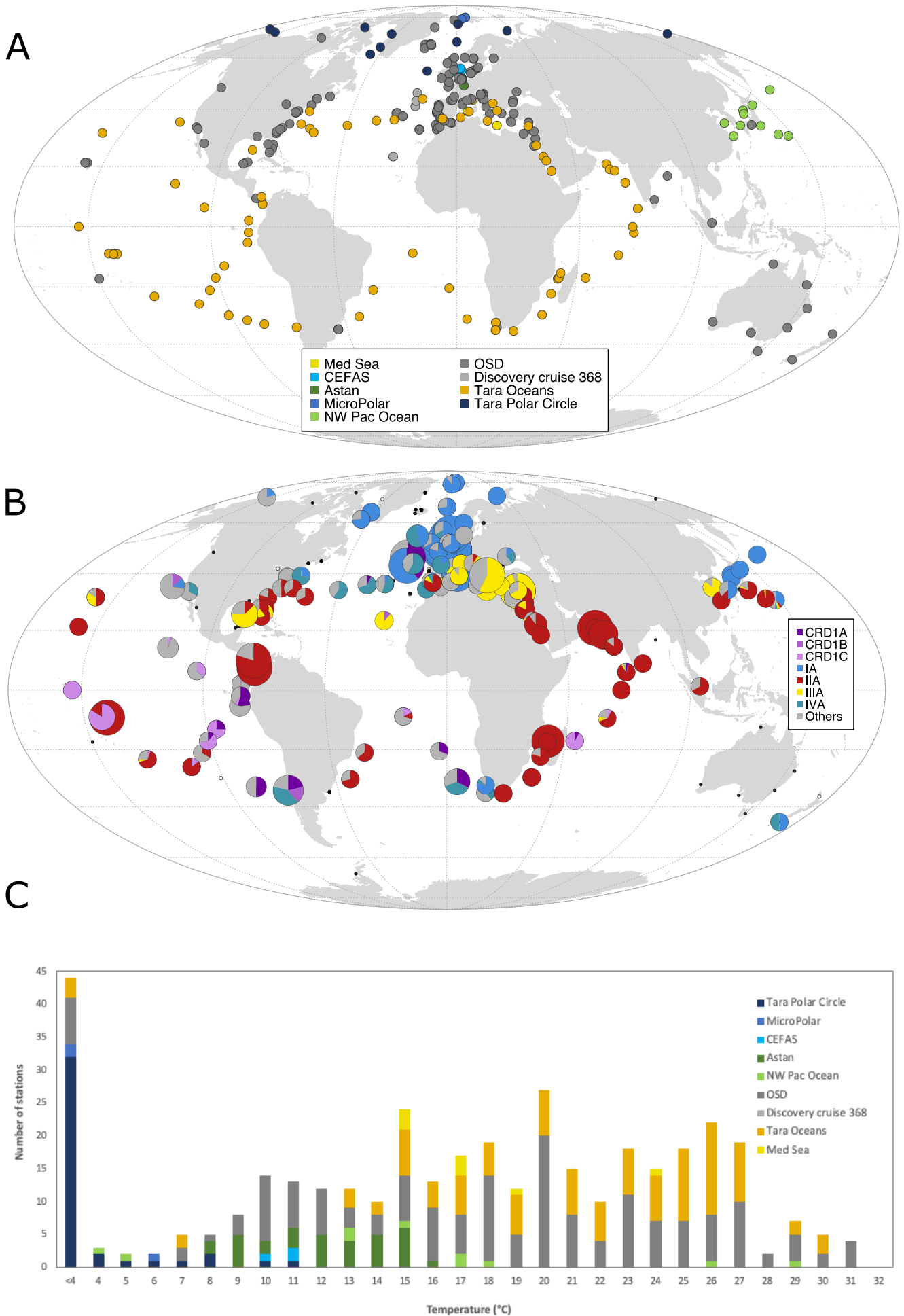
Supplementary Figure 2. Oceanwide environmental data used in this study to determine the environmental realized thermal niches of the main ESTUs from clades CRD1 and I to IV. **(A)** Map of the sampling sites, **(B)** Relative abundance of *Synechococcus* ESTUs IA to IVA and CRD1A to C. **(C)** Temperature distribution of the sampling sites. The inserts specify **(A,C)** the name of campaigns or datasets analyzed and **(B)** the *Synechococcus* ESTUs.
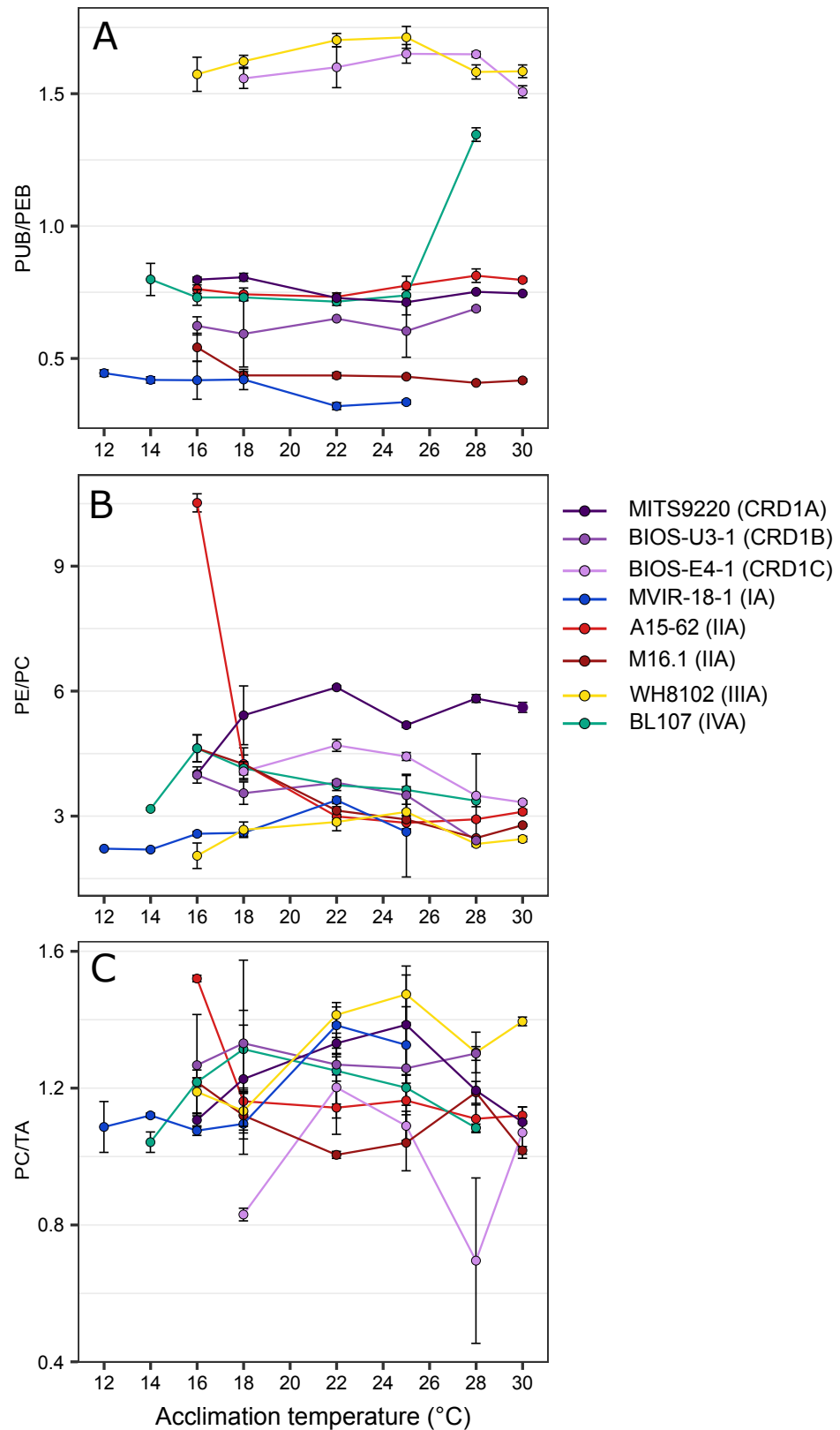
A. RpcA

B. RpcB
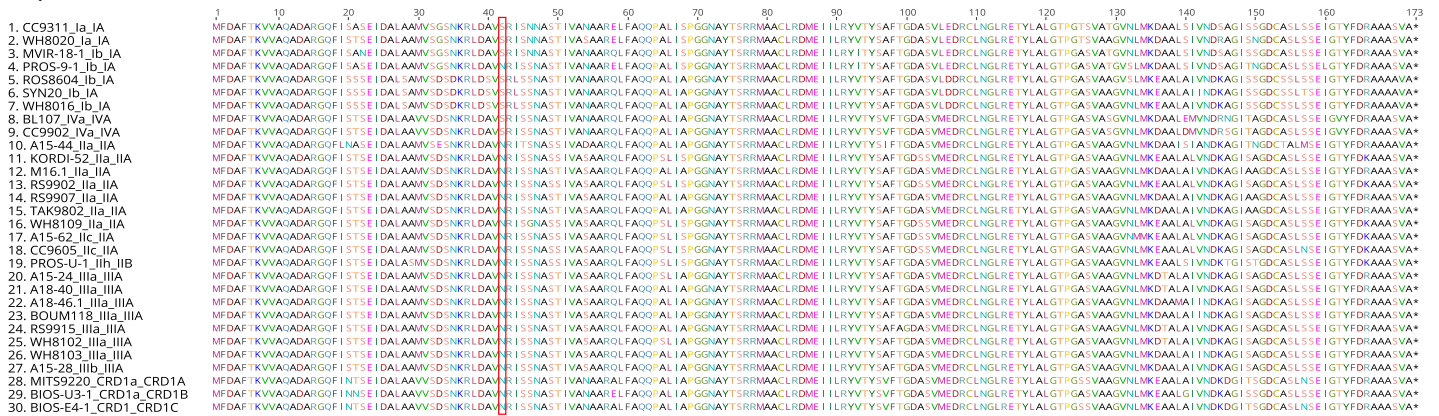
Supplementary Figure 3. Alignment of RpcA and RpcB, encoding phycocyanin α- and β-subunits, from CRD1 and clades I-IV *Synechococcus* strains. (A) RpcA. (B) RpcB. Substitutions potentially involved in thermotolerance are shown by a red rectangle in the alignment.

Supplementary Figure 4. Variation with growth temperature of phycobilins and phycobiliproteins fluorescence excitation and emission ratios. (A) Average PUB:PEB ratios. (B) Average phycoerythrin (PE) to phycocyanin (PC) ratios. (C) Average PC to terminal acceptor (TA) ratios. The insert indicates the strain names, their corresponding ESTU (sensu Farrant et al., 2016) and pigment type (sensu Humily et al., 2013) between brackets.
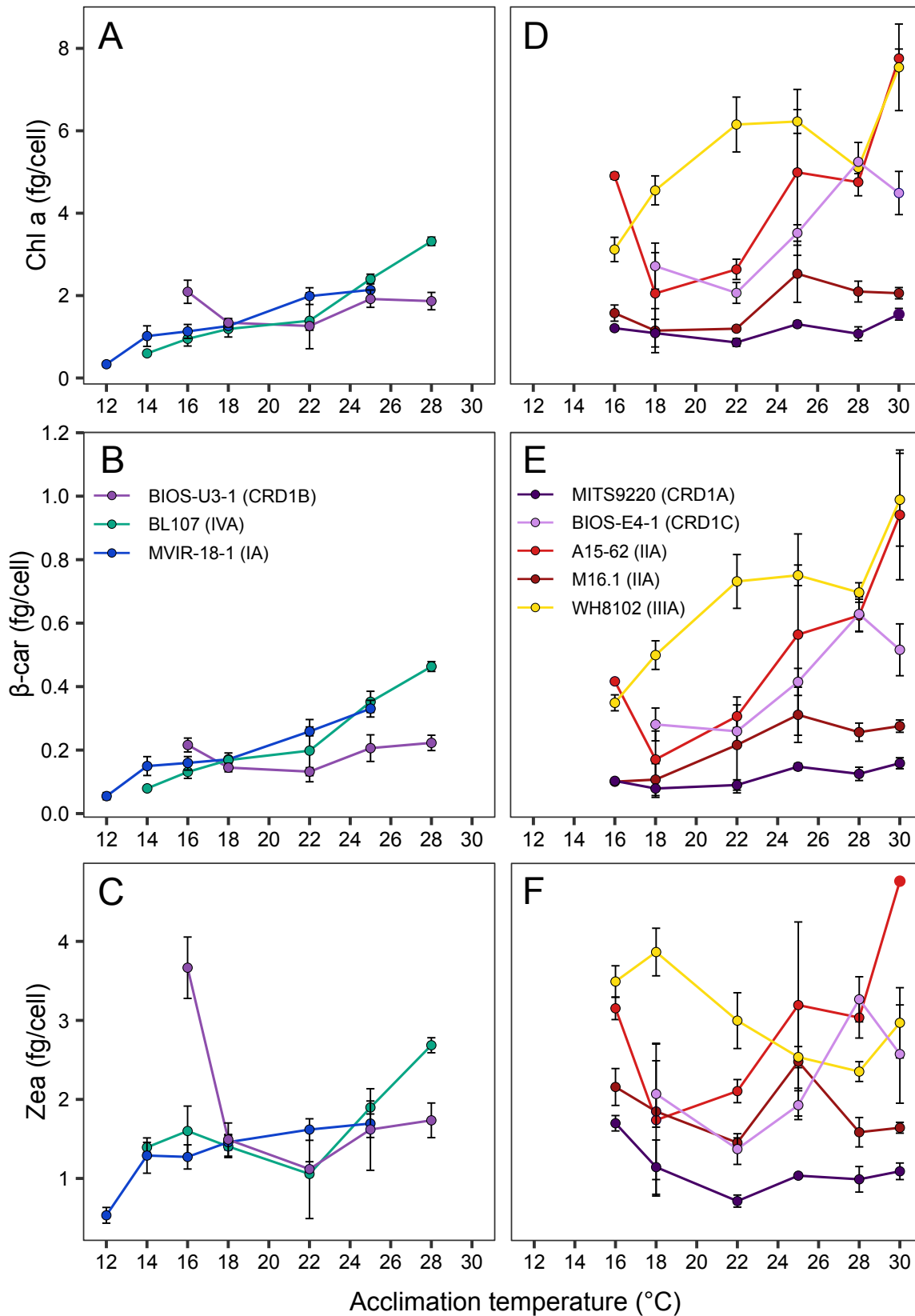
Supplementary Figure 5. Variation with growth temperature of the three main liposoluble pigments per cell for CRD1 vs. clade I and IV strains. (A, D) Chlorophyll (Chl) a content (fg/cell). **(B, E)** Zeaxanthin (Zea) content (fg/cell). **(C, F)** β-carotene (β-car) content (fg/cell). **(A-C)** CRD1-B strain BIOS-U3-1 vs. cold thermotypes. **(D-F)** CRD1-A strain MITS9220 and CRD1-C strain BIOS-E4-1 vs. warm thermotypes. Inserts indicate the strain names and their corresponding ESTU (*sensu* Farrant et al., 2016) between brackets.
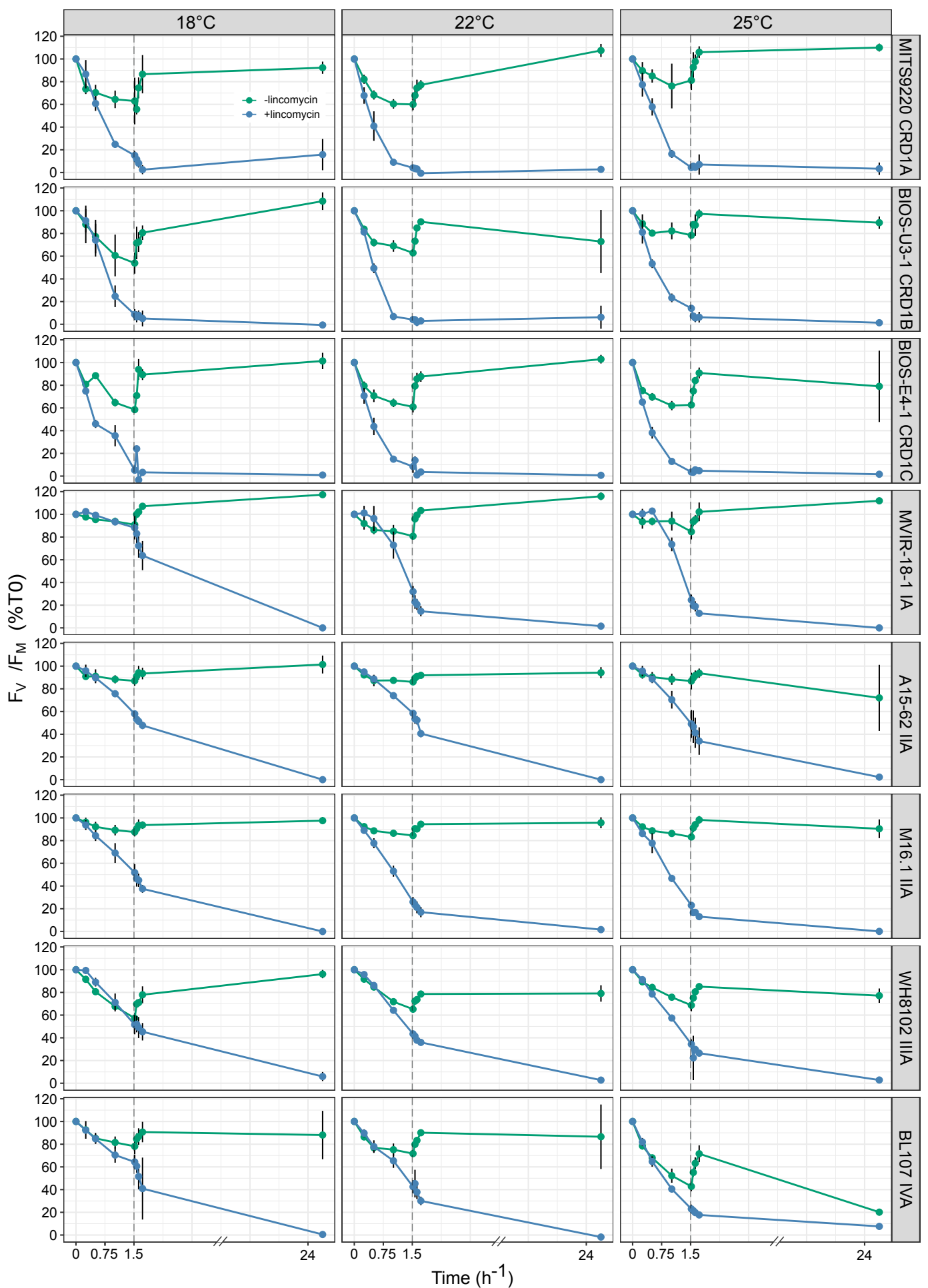
Supplementary Figure 6. Time course of photosystem II quantum yield (F_V/F_M) following light stress in the presence or absence of lincomycin for CRD1 and clade I-IV strains acclimated to different temperatures. Cultures acclimated to 75 µE m^{-2} s^{-1} were shifted to 375 µE m^{-2} s^{-1} at T0 for 90 min, then shifted back to the initial light conditions for 24h as indicated by a vertical dashed line on each figure. Strain names and their corresponding ESTU between brackets (*sensu* Farrant et al., 2016) are indicated on the right hand side, acclimation temperature are indicated on the top, whilst line colour indicates the lincomycin treatment (i.e. -/+ linco).